Acta Pharmaceutica Sinica B 2024;14(2):729−750

Chinese Pharmaceutical Association
Institute of Materia Medica, Chinese Academy of Medical Sciences

Acta Pharmaceutica Sinica B

www.elsevier.com/locate/apsb
www.sciencedirect.com

ORIGINAL ARTICLE

Trilogy of drug repurposing for developing cancer and chemotherapy-induced heart failure co-therapy agent

Xin Chen[a,c,†], Xianggang Mu[a,†], Lele Ding[b,†], Xi Wang[b,†], Fei Mao[a], Jinlian Wei[a], Qian Liu[b], Yixiang Xu[a], Shuaishuai Ni[b,*], Lijun Jia[b,*], Jian Li[a,*]

[a]*State Key Laboratory of Bioreactor Engineering, Shanghai Frontiers Science Center of Optogenetic Techniques for Cell Metabolism, Frontiers Science Center for Materiobiology and Dynamic Chemistry, Shanghai Key Laboratory of New Drug Design, School of Pharmacy, East China University of Science and Technology, Shanghai 200237, China*
[b]*Cancer Institute, Longhua Hospital, Shanghai University of Traditional Chinese Medicine, Shanghai 200032, China*
[c]*College of Pharmacy, Jinan University, Guangzhou 510632, China*

Received 9 July 2023; received in revised form 5 October 2023; accepted 26 October 2023

KEY WORDS

Anticancer;
Heart failure;
Complication;
Drug repurposing;
Bi-functional drug

Abstract Chemotherapy-induced complications, particularly lethal cardiovascular diseases, pose significant challenges for cancer survivors. The intertwined adverse effects, brought by cancer and its complication, further complicate anticancer therapy and lead to diminished clinical outcomes. Simple supplementation of cardioprotective agents falls short in addressing these challenges. Developing bi-functional co-therapy agents provided another potential solution to consolidate the chemotherapy and reduce cardiac events simultaneously. Drug repurposing was naturally endowed with co-therapeutic potential of two indications, implying a unique chance in the development of bi-functional agents. Herein, we further proposed a novel "trilogy of drug repurposing" strategy that comprises function-based, target-focused, and scaffold-driven repurposing approaches, aiming to systematically elucidate the advantages of repurposed drugs in rationally developing bi-functional agent. Through function-based repurposing, a cardioprotective agent, carvedilol (CAR), was identified as a potential neddylation inhibitor to suppress lung cancer growth. Employing target-focused SAR studies and scaffold-driven drug design, we synthesized 44 CAR derivatives to achieve a balance between anticancer and cardioprotection. Remarkably,

*Corresponding authors.
E-mail addresses: nss1106@126.com (Shuaishuai Ni), ljjia@shutcm.edu.cn (Lijun Jia), jianli@ecust.edu.cn (Jian Li).
[†]These authors made equal contributions to this work.
Peer review under the responsibility of Chinese Pharmaceutical Association and Institute of Materia Medica, Chinese Academy of Medical Sciences.

https://doi.org/10.1016/j.apsb.2023.11.004

optimal derivative **43** displayed promising bi-functional effects, especially in various self-established heart failure mice models with and without tumor-bearing. Collectively, the present study validated the practicability of the "trilogy of drug repurposing" strategy in the development of bi-functional co-therapy agents.

1. Introduction

Cancer survivors, who live for five years or more after their initial cancer diagnosis, always suffer a diverse and complex set of complications. Clinical statistics from the National Cancer Institute (NCI, USA) revealed that approximately 80% of cancer survivors experiencing chronic adverse health conditions, disorders, or damage to organs and nerves (Fig. 1A)[1]. Among these complications, cardiovascular (CV) diseases (CVD), such as left ventricular (LV) dysfunction (LVD) and heart failure (HF), now represented the second leading cause of long-term morbidity and mortality among cancer survivors[2–4]. The underlying cause is thought to be the late effects of conventional chemotherapy and targeted therapy[2,5]. A wide range of anticancer agents, including anthracyclines, proteasome inhibitors, histone deacetylase inhibitors, kinase inhibitors, and macromolecule drugs, come at a cost in adverse cardiac events[5–8]. Furthermore, frequently using multiple anticancer drugs further exacerbates the incidence of cardiac events. Previous attempts to decrease the chemotherapy side effects, have focused on chemical and physical modification strategies, such as prodrugs and nano-cargoes. However, these approaches have encountered limitations related to druggability, release conditions, and metabolic stability[9,10]. Meanwhile, clinical administration pays attention to balancing reducing cardiac events and cancer treatment for providing optimal anticancer efficacy[11,12]. Cancer survivors are often advised to take cardioprotective agents by either individually or combination, such as dexrazoxane, β-blockers, and "statin" drugs, during the intermission of chemotherapy cycles[5]. However, maintaining this delicate balance becomes challenging due to factors such as continuous body weakness, tumor progression, and drug resistance. Therefore, we would be to explore whether the development of bi-functional agents with both cardioprotective and anticancer efficacy was a practicable strategy to reduce cardiac events while enhancing chemotherapy effectiveness.

In this study, the first challenge was to identify an ideal lead compound with bi-functional properties. Drug repurposing is a classical method to discover new functions outside the scope of the original indication for approved drugs[13,14]. However, the inherent bi-functional characteristics of repurposed drugs have often been neglected by previous studies. The present study first investigated the repurposing potential of 992 non-anticancer FDA-approved drugs in-house, revealing that up to 17.8% of agents (176/992) displayed potential antitumor activities (Fig. 1B). Especially, over one fourth of cardiovascular agents (49/193) were reported to affect tumor growth (Fig. 1B, Supporting Information Table S1), suggesting that it was feasible to develop a bi-functional agents from cardiovascular agents. To further address the challenge, we proposed a novel "trilogy of repurposing" strategy in this study, which divided the entire process of drug repurposing into three sequential procedures: function-based, target-focused, and scaffold-driven repurposing (Fig. 1C).

The concept of "function-based repurposing" involves discovering and validating new therapeutic function and its associated interactive mechanism of repurposed drugs, similar to classical drug repurposing. Target-focused repurposing puts the scope to elucidate the bi-functional and structural relationship between the original target (on-target) and the newly discovered target (off-target) of the repurposed drug. Scaffold-driven repurposing aims to enhance new functional efficacy while maintaining the original efficacy through structural modification of the repurposed drug. In the process of "function-based repurposing", we identified carvedilol (CAR), a β-adrenergic receptor (β-AR) blocker clinically used for cardioprotection, as a bi-functional molecule capable of suppressing lung cancer growth by targeting the neddylation pathway. Dependent on the target-focused and scaffold-driven SAR studies, we designed and synthesized a series of CAR derivatives to achieve a balanced bi-functional efficacy of anticancer and cardioprotection.

2. Materials and methods

2.1. Synthesis and characterization of 3–44

The details of the synthesis and characterization of **3–44** employed in this manuscript are described in the Supporting Information.

2.2. AlphaScreen approach

The protein Nedd8, NAE, UBE2M, Rbx1/CUL1^{CTD} were prepared that was a gift from Prof. Jin Huang, Shanghai Jiao Tong University School of Medicine, China. The protocol and screening process were applied and guided by Prof. Yi Sun, Zhejiang University School of Medicine, China[15,16]. In the AlphaScreen competitive inhibition assay for the Nedd8/cullin1 PPI, 10 μmol/L of C-terminally biotinylated Nedd8 and 1 μmol/L of N-terminally His6-tagged Rbx1/CUL1^{CTD} were mixed into an assay buffer of 50 mmol/L Tris-HCl (pH = 7.4), 5 mmol/L $MgCl_2$, 0.5 mmol/L DTT, 0.1 mg/mL BSA, along with the initiators of 25 nmol/L NAE, 1 μmol/L UBE2M, and 100 μmol/L tested compound (193 cardiovascular drugs) at 25 °C for 15 min, 10 μmol/L MLN4924 as a positive control. 2 mmol/L ATP were added in 20 μL of assay buffer. The assay plates were covered black and gently mixed on an orbital shaker at 4 °C for 45 min. The streptavidin-coated donor beads and the nickel chelate acceptor beads were added to a final concentration of 10 μg/mL in 25 μL assay buffer. The mixture was incubated for 2 h at 25 °C before detection. The results analysis was determined by GraphPad Prism 7.0.

2.3. *Cell culture and reagents*

Human lung cancer cell lines A549 and H1299, human liver cancer cell lines HepG2 and Huh7, human breast cancer cell lines T-47D and MB231, human colon cancer cell line SW480, rat cardiac myoblast H9c2, were obtained from the American Type Culture Collection (Manassas, VA, USA) and Institute of Biochemistry and Cell Biology (CAS, Shanghai), passaged five to six times before use. Cells were cultured in Dulbecco's modified Eagle's medium (Hyclone, Logan, UT, USA), containing 10% fetal bovine serum (Biochrom AG, Berlin, Germany) and 100 units/mL penicillin/streptomycin solution and maintained in a

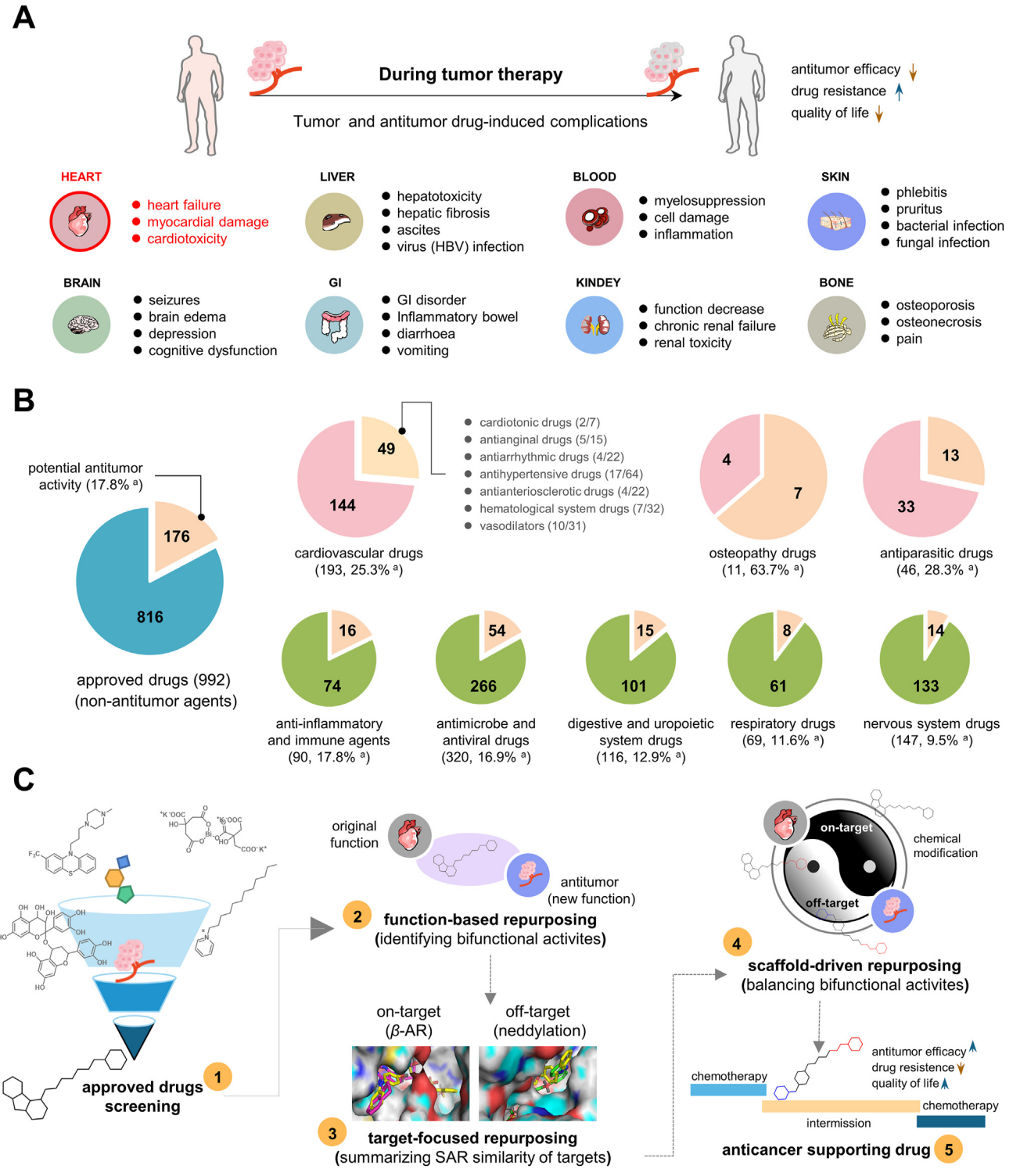

Figure 1 Trilogy of drug repurposing is a potential strategy for antitumor supportive therapy. (A) Representative tumor complications. (B) Potential anticancer structures and their proportion in approved drugs. [a]Rate of potential anticancer structures in respective types. (C) Schematic diagram of trilogy of drug repurposing in the presence of study.

humidified atmosphere of 5% CO_2 at 37 °C (standard culture conditions). MLN4924, CAR, and CAR derivatives were dissolved in dimethyl sulfoxide (DMSO) and kept at −20 °C for *in vitro* studies. MLN4924, CAR, or **43** were dissolved respectively in 5% 2-hydroxypropyl-β-cyclodextrin and 5% castor oil (Macklin Reagent, Shanghai, China), while doxorubicin (DOX) was dissolved in saline *in vivo* studies. The solution of tested agents was freshly made every day when was used.

2.4. Enzyme-based neddylation activity assay

0.5 μL NAE (final concentration, 1 μmol/L), 0.4 μL Nedd8 (final concentration, 10 μmol/L), 0.4 μL UBE2M (final concentration, 1 μmol/L), 0.7 μL RBX1/$CUL1^{CTD}$ (final concentration, 1 μmol/L), 0.5 μL Tris-HCl (1 mol/L, pH = 7.4), 0.5 μL $MgCl_2$ (0.1 mol/L), 0.5 μL DTT (10 mmol/L), 0.1 μL 0.1 mg/mL BSA, 1.4 μL ddH_2O, were added into in each well of 96-well plates, followed with 1.0 μL water solution (<0.5% DMSO) of MLN4924 (final concentration, 10 μmol/L) or CAR (final concentration, 3.6, 11, 33, 100, 300 μmol/L) in order. 2.0 μL (final concentration, 20 μmol/L) ATP was added to the reaction after the mixture was incubated for 15 min at 25 °C. The mixture was incubated at 37 °C for 30 min. The reaction was quenched by the addition of 2 μL EDTA (1 mol/L), and protein samples was electrophoresed under non-reducing conditions on a 12.5% SDS-PAGE gel. UBE2M−Nedd8 and $CUL1^{CTD}$−Nedd8 levels were determined by Western blot analysis. In respect of the ATP-competitive assay, the concentration of CAR (final concentration, 50 μmol/L) and ATP (final concentration, 0.05, 0.1, 0.5, 1 mmol/L) were changed, all else being equal as above.

2.5. Cell-based neddylation activity assay

Either A549 or H1299 cells were exposed to the indicated concentrations of MLN4924 (1 μmol/L), CAR (10, 20, 40, 60 μmol/L), or **43** (1.3, 2.5, 5, 10 μmol/L), and 0.1 % (*v*/*v*) DMSO as a control group for 24 h, respectively. Cells were washed three times with ice-cold PBS, resuspended in RIPA lysis buffer, and incubated on the ice for 30 min. Cell debris was removed by centrifugation at 15,000 rpm for 10 min at 4 °C. The protein concentration of the supernatant was determined with a Thermo Fisher protein assay dye reagent (Thermo Fisher). Equal protein amounts (5−10 μL) were electrophoresed on SDS-PAGEs and subjected to Western blot analysis as follows. Equal amounts of each sample were mixed with 2 × SDS-PAGE Protein Loading Buffer (YEASEN, 20315ES05), denatured by heating at 95 °C for 10 min, then were separated by 8%−15% PAGE Gel Quick Preparation Kit (YEASEN, 20324ES62) and transferred to PVDF membrane. The membrane was blocked using 5% nonfat dry milk for 1 h at room temperature, followed by overnight incubation at 4 °C with antibodies against target proteins: NEDD8 (Cell Signaling Tec, 2745), CUL1 (Abcam, ab75817), CUL2 (Abcam, ab166917), CUL3 (Abcam, ab108407), CUL4A (Abcam, ab72548), CUL5 (Abcam, ab184177), cleaved-PARP (Cell Signaling Tec, 5625), cleaved-Caspase3 (Cell Signaling Tec, 9661), β-actin (Cell Signaling Tec, 3700). Next, the membrane was incubated with species-specific HRP-conjugated secondary antibody (anti-rabbit IgG antibody, CST, 7074P2; Goat anti-mouse IgG antibody, Arigo, ARG65350). The protein bands were visualized using a chemiluminescence imaging system (Tanon4600SF). Each experiment was performed in triplicate.

2.6. Cell proliferation and cell clonogenic assays

For evaluating the proliferation of cultured cells, cells seeded (A549, H1299, HepG2, Huh7, T-47D, MB231, SW480) in 96-well plates with 1500−2500 cells per well (the absorption value at 1.5−2.5), in triplicate, and cultured overnight were treated with CAR or CAR derivative for 72 h, followed by cell counting kit-8 (CCK-8) assay. The absorbance of each well at 450 nm was recorded using a Microplate Reader (Bio-Tek Instruments, Synergy H1). Cell viability was evaluated by measuring the absorbance and calculated by Eq. (1):

$$\text{Cell viability} = (OD_{positive} - OD_{control}) / (OD_{negative} - OD_{control}) \quad (1)$$

For clonogenic assays, cells (A549 and H1299) were seeded in six-well plates (150 cells per well, respectively) in triplicate, and were treated with MLN4924 or other drugs and cultured for 10−14 days. The colonies of control groups were considered as around 50 cells or more and counted. Representative results of three independent experiments with similar trends were presented.

2.7. Cell apoptosis assay

Apoptosis was evaluated using a FITC annexin V apoptosis detection kit. A549 cells were seeded at 2.5×10^5 cells per well in 6-well plates and allowed to attach overnight. Cells were treated with different concentrations of either CAR (10, 20, 40 μmol/L) or **43** (1.1, 3.3, 10 μmol/L), and 0.1% (*v*/*v*) DMSO as a control group for 72 h. Cells were dissociated using trypsin, then were washed three times with ice-cold PBS and resuspended in 100 μL 1 × binding buffer, followed with the addition of 5 μL FITC annexin V staining solution and 5 μL PI staining solution. After incubation at room temperature in the dark for 15 min, another 400 μL 1 × binding buffer was added. Stained cells were analyzed immediately by flow cytometry.

2.8. Cell cycle arrest assay

A549 cells treated with DMSO or various concentrations of agent CAR (10, 20, 40 μmol/L) were harvested and fixed in 90% ethanol at −20 °C for 24 h, then centrifuged at 1500 rpm for 10 min at 4 °C in tubes. The residue in each tube was washed three times with ice-cold PBS, and stained with 0.5 mL propidium iodide solution (36 μg/mL; Sigma, St. Louis, MO, USA) contained RNase A (10 μg/mL; Sigma) at 37 °C for 30 min, and analyzed for cell−cycle profile with Flowjo. Representative results of three independent experiments with similar trends are presented.

2.9. Molecular modeling

The X-ray structure of either NAE or β-AR was downloaded from the Protein Data Bank (PDB ID: 3GZN of NAE; PDB ID: 6PS3 of β-AR). Crystallographic water, ligands, and alternate conformations were removed by using the protein preparation protocol in Gold 5.0. The docking procedure of tested agents was performed by employing the DOCK program in Gold 5.0, and the structural image was obtained using PyMOL software.

2.10. Cardiac injury assays

2.10.1. DOX-induced injury model

Cultured H9c2 cells were trypsinized and replated in 96-well plates at a density of 8000 cells per well. DOX at the concentration of 25 nmol/L was added to the cells for 6 h. After incubation, the medium was removed, and the cells were washed with ice-cold PBS. Then, DMEM with 10% fetal bovine serum was added to the DOX-induced injury model. Subsequently, compounds **40**, **43**, and CAR at the concentration of 1 μmol/L were added individually to the cells for 12 h and washed with PBS. The viability of cardiomyocytes was determined at 450 nm using CCK-8 assay.

2.10.2. H/R injury model

Cultured H9c2 cells were trypsinized and replated in 96-well plates at a density of 8000 cells per well. Compounds at the concentration of 1 μmol/L were added individually to the cells and moved into the hypoxia chamber (95% N_2 and 5% CO_2) for 6 h. After incubation, the medium was removed, and the cells were washed with ice-cold PBS. Then, DMEM with 10% fetal bovine serum was added to the hypoxia injury cells and incubated in normal conditions for reoxygenation of 12 h. The viability of cardiomyocytes was determined at 450 nm using CCK-8 assay.

2.10.3. GD injury model

Cultured H9c2 cells were trypsinized and replated in 96-well plates at a density of 8000 cells per well. Compounds at the concentration of 1 μmol/L were added individually to the cells prior to GD for 12 h. After incubation, the medium was removed, and the cells were washed with ice-cold PBS. Then, DMEM without glucose and fetal bovine serum was added for co-incubating for 6 h to induce cell injury. The viability of cardiomyocytes was determined at 450 nm using CCK-8 assay.

2.11. In vivo evaluation assays

The animals were housed under specific pathogen-free conditions with a 12 h light−dark cycle at a temperature of 25 °C, humidity of 55%, and free access to water and food. Animal experiments were performed in accordance with the National Guidelines for Experimental Animal Welfare, with approval from the Institutional Animal Care and Use Committee of Longhua hospital, Shanghai University of Traditional Chinese Medicine (PZSHUTCM2302270021).

2.11.1. A549 xenograft growth mice model to evaluate the anticancer efficacy of CAR

Female nude mice were subcutaneously injected with 2×10^6 A549 cells in 100 μL PBS according to protocols of tumor transplant research. After tumor induction and growth at 30−80 mm^3 (about 7 days), nude mice were divided into four groups randomly, including the control group (10% 2-hydroxypropyl-β-cyclodextrin/water solution), MLN4924-treated positive group (60 mg/kg), and two CAR-treated groups (15 and 30 mg/kg). All groups were administrated by intraperitoneal injection and were treated with one dose per day and per five-day treatment with a two-day rest as the treatment cycle. Body weights and tumor volumes were measured every 3 days. On the 24th day after inoculation, all the mice were sacrificed (tumor volume >1000 mm^3). Tumor volumes and mass were measured for each group.

2.11.2. A549 xenograft growth mice model to evaluate the anticancer efficacy of 43

Female nude mice were subcutaneously injected with 1×10^6 A549 cells in 100 μL PBS according to protocols of tumor transplant research. After tumor induction and growth at 30−80 mm^3 (about 7 days), nude mice were divided into five groups randomly, including control group (10% 2-hydroxypropyl-β-cyclodextrin/water solution), DOX-treated positive group (2 mg/kg), CAR-treatment as the other positive group (30 mg/kg), and two **43**-treated groups (5 and 20 mg/kg), and were administrated by intraperitoneal injection. Herein, the DOX-treated group was administrated with two doses per week, the other groups are one dose per day, and per five-day treatment with a two-day rest as the treatment cycle. Body weights and tumor volumes were measured every 3 days. On the 30th day after the treatment, all the mice were sacrificed (tumor volume >1000 mm^3). Tumor volumes and mass were measured for each group.

2.11.3. DOX-induced HF C57 mice model

Except for the sham group treated with saline, other C57 mice were pretreated with one dose of 4 mg/kg of DOX per week. After three weeks, these DOX-treated mice were divided into three groups randomly, including the vehicle group (saline), the CAR-treated positive group (10 mg/kg), and **43**-treated group (10 mg/kg). All groups were administrated by intraperitoneal injection, and were treated with one dose per day for another three weeks, and per five-day treatment with a two-day rest as the treatment cycle. Body weights were measured every 3 days. Subsequently, all the mice were tested by observing the M-mode echocardiograms.

2.11.4. A549 bearing DOX-induced HF nude mice model

Female nude mice were subcutaneously injected with 1×10^6 A549 cells in 100 μL PBS according to protocols of tumor transplant research. After tumor induction and growth at 30−80 mm^3 (about 7 days), nude mice were divided into seven groups randomly, including control group (10% 2-hydroxypropyl-β-cyclodextrin/water solution), DOX-treated group (3 mg/kg), two **43**-treated groups (10 and 20 mg/kg) by the intraperitoneal administration, one **43**-treated group (20 mg/kg) by the oral administration, two combination-treated groups (DOX + **43**) with the same doses as the single treatment ones that were performed with a metronomic schedule. Herein, the DOX-treated group was administrated one dose per week, the other groups are three doses per week, and per six-day treatment with a one-day rest as the treatment cycle. Body weights and tumor volumes were measured every 3 days. On the 30th day after the treatment, all the mice were terminated with the treatment of agents (tumor volume >1000 mm^3). Then, mice were trained by the rotarod and grip tests for five days (qd), 30 min per day, to evaluate the movement function.

2.11.5. Advanced A549 bearing DOX-induced HF nude mice model

Female nude mice were subcutaneously injected with 1×10^6 A549 cells in 100 μL PBS according to protocols of tumor transplant research. After tumor induction and growth at 150−200 mm^3 (about two weeks), nude mice were divided into four groups randomly, including the control group (10% 2-hydroxypropyl-β-cyclodextrin/water solution), DOX-treated group (2 mg/kg), **43**-treated groups (10 mg/kg), one combination-treated group (DOX + **43**) with the same doses as the single treatment ones that were performed with a metronomic schedule, by the intraperitoneal

administration. Herein, the DOX-treated group was administrated with one dose per week, the other groups are two doses per week, and per five-day treatment with a two-day rest as the treatment cycle. Body weights and tumor volumes were measured every 3 days. On the 21st day (three weeks) after the treatment, all the mice were terminated with the anticancer evaluation (tumor volume $>1000\ mm^3$). Then, mice were trained by the grip tests for five days (qod), 30 min per day, to evaluate the movement function. Subsequently, all the mice were tested by observing the M-mode echocardiograms.

3. Results

3.1. *Cardioprotective CAR suppresses lung cancer growth in vitro and in vivo*

Protein neddylation is a posttranslational modification of conjugating the neuronal precursor cell expressed developmentally down-regulated protein 8 (Nedd8) to substrates[17,18]. This process goes through an ATP-dependent three-step enzymatic cascade reaction by E1 (NAE), E2s (UBE2M/2F), and E3s (*e.g.*, ROC1/2), ultimately transferring Nedd8 to specific substrates, including members of the cullin family (*e.g.*, CUL1, 2, 3, 4a, 4b, and 5) (Supporting Information Fig. S1A)[19,20]. Previous studies have revealed that the neddylation pathway is overexpressed in various human lung cancers and correlates with the disease progression, while pharmacological targeting of this pathway has emerged as an attractive therapeutic strategy[21,22]. Several neddylation inhibitors have been discovered in recent years, such as MLN4924, complex 1 and M22 (Fig. S1B)[23–25]. MLN4924, known as a neddylation inhibitor by targeting NAE, had already entered phase III clinical trials.

In this study, 193 aforementioned cardiovascular drugs were initially explored for the potential by conducting an AlphaScreen approach, and 14 agents had over 80% neddylation inhibitory rates (Supporting Information Fig. S2A)[15]. Subsequently, we evaluated the antiproliferation activities of these ten hit compounds (Fig. S2B). Herein, four hit compounds displayed acceptable antiproliferation activities (cell viability <50% @ 100 μmol/L), including CAR, azelnidipine, bevantolol and nicardipine. Meanwhile, we evaluated the neddylation inhibitory activities of these ten agents (Fig. S2C), and identified that CAR and bevantolol presented promising neddylation inhibitory activities in A549 cells, at their respective concentrations. In this study, CAR was chosen as a bi-functional leading compound for further investigating, due to its more comprehensive performance and clinical application for cardioprotection[5,26] (Fig. 2A). CCK-8 assay showed that CAR inhibited the proliferation of various cancer cell lines (IC_{50} = 20−80 μmol/L, Supporting Information Fig. S3A), especially against the lung cancer cell lines A549 (IC_{50} = 22.9 ± 0.2 μmol/L) and H1299 (IC_{50} = 32.4 ± 0.5 μmol/L) (Fig. 2B). CAR also completely inhibited the clonogenic survival of either A549 or H1299 cells at the concentration of 30 μmol/L (Fig. 2C, D). The inhibition of neddylation pathway can induce cancer cells apoptosis and cycle arrest[27]. Hence, an Annexin-V/PI double staining assay was performed for evaluating the capacity of CAR to induce apoptosis. The results showed that the total numbers of early and late apoptotic cells significantly elevated in a dose-dependent manner in A549 and H1299 cells (Fig. S3B−S3E). In addition, two classical apoptosis markers cleaved-PARP and cleaved-caspase3 were accumulated in the CAR-treated A549 cells (Fig. S3F). The results of DNA content of cell nuclei showed that CAR induced the cycle arrest of A549 cells at the G_1 phase (Supporting Information Fig. S4). Considering that targeting neddylation can sensitize various chemotherapy[28,29], our present study verified the potential synergistic anticancer effect of CAR with either DOX or HDAC inhibitor entinostat (ENT) by a classical checkboard test (Fig. 2E, F). Moreover, these two chemotherapeutics led to severe cardiovascular disease as mentioned above. In general, the combination of CAR and DOX displayed a moderate synergistic effect, and the combination of CAR and ENT displayed a better synergistic effect than that of CAR and DOX (Supporting Information Fig. S5).

Then, an A549 xenograft growth mice model was conducted to evaluate the anticancer efficacy of CAR, along with the synergistic anticancer effect of CAR and ENT combination. Herein, six different regimens, including control group, MLN4924-treated group (30 mg/kg) as the positive control, two CAR-treated groups (15 or 30 mg/kg), ENT-treated group (10 mg/kg) and the combination group of CAR (15 mg/kg) and ENT (10 mg/kg), were performed for an anticancer therapy. The indicated agents were administrated for 5 day as a cycle by the intraperitoneal injection. High dose (30 mg/kg) of CAR-treated group displayed better tumor growth inhibition (TGI) percentage (TGI = 36.4%) than mock group and low dose (15 mg/kg) of CAR-treated group, which was comparable with the MLN4924-treated group (Fig. 2G−J). Moreover, CAR significantly sensitized the anticancer efficacy of ENT without resulting in the mice weight loss. All these results showed that CAR was repurposed in suppressing the tumor growth *in vitro* and *in vivo*.

3.2. *CAR is a potential neddylation inhibitor*

An enzymatic assay was primarily performed to evaluate the cullin1−Nedd8 adduct by incubating with the progressive concentrations of CAR, then showed that CAR inhibited the cullin1 neddylation in a dose-dependent manner (Fig. 3A). As mentioned above, the cullin family is consist of multiple cullin subunits that are regulated as major substrates by the neddylation pathway. Herein, subunits cullin1, 2, 3 and 4 (CUL1, 2, 3, 4) are modified by Nedd8 *via* the NAE−UBE2M−ROC1 axis, while the formation of cullin5 (CUL5)−Nedd8 adduct is regulated by the NAE−UBE2F−ROC2 axis (Supporting Information Fig. S6). In the present study, CAR not only inhibited the levels of CULs−Nedd8 adducts without affecting the levels of NAE1 (Fig. 3B, C; and Supporting Information Fig. S7A), but also decreased the global Nedd8 modification in A549 and H1299 cells (Fig. 3D and Fig. S7B). NAE activates Nedd8 in an ATP-dependent manner, while targeting the ATP-binding pocket of NAE can inhibit the function of NAE[30]. The ATP rescuing assay *in vitro* showed that the levels of CUL1−Nedd8 and UBE2M−Nedd8 adduct were elevated with the increase of ATP concentrations (Fig. 3E).

Moreover, the scaffold of CAR can be divided into three moieties, including a carbazole group, an oxy-1,2-propanolamine for adrenoceptor agonists, and a side chain that is composed of an ethoxyl linker chain and a catechol ether. An additional molecular docking study was conducted to investigate the binding mode between the structure of CAR and potential target NAE by comparison with MLN4924 (Fig. 3F, G; and Supporting Information Fig. S8A). In general, CAR formed multiple H-bonds with the amino acid residues of NAE as same as MLN4924, especially at the position of *iso*-propanolamine moiety, such as D167, G76, and R111. Collectively, these results suggested that CAR might target NAE to inhibit the neddylation pathway.

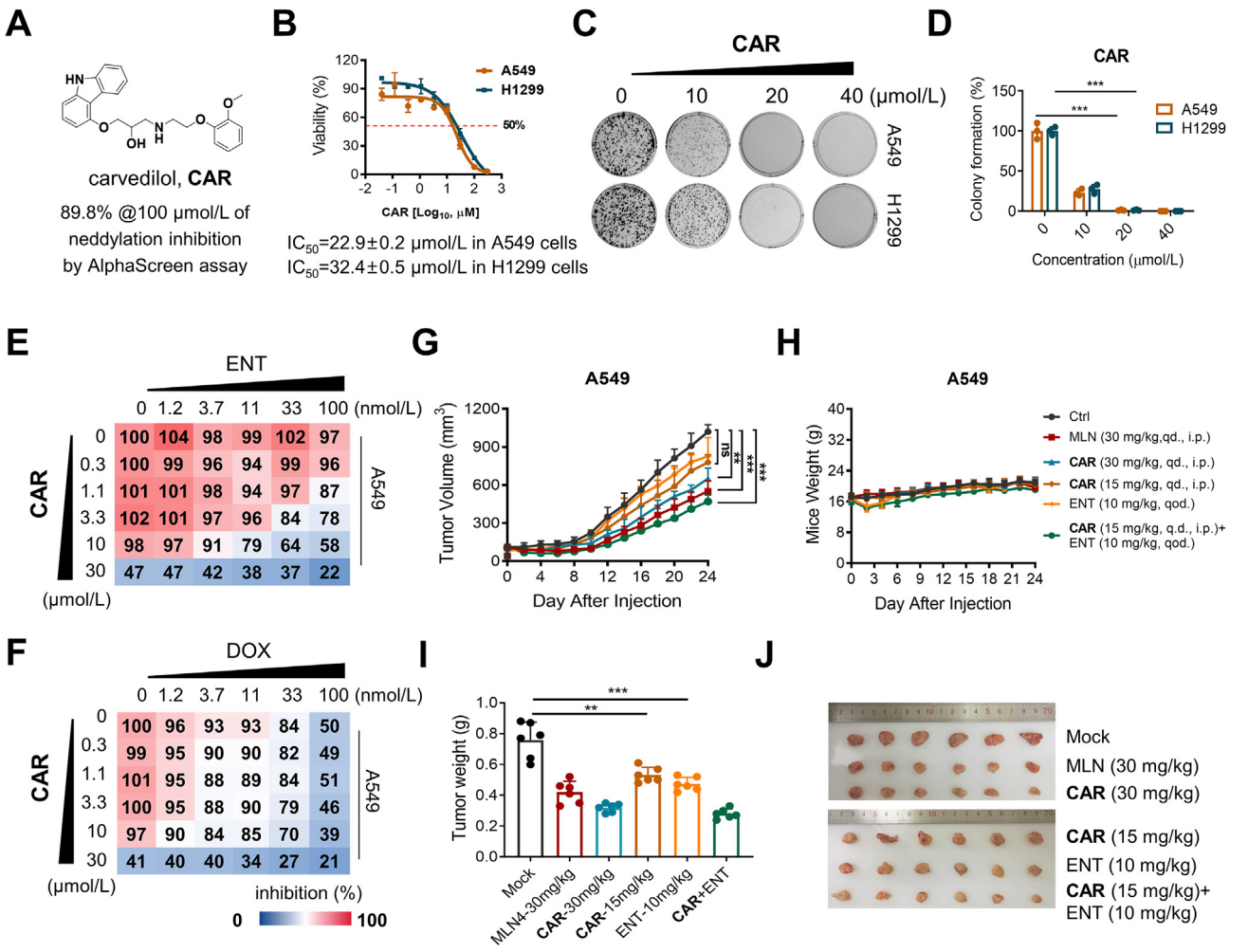

Figure 2 Function-based repurposing validated the antitumor activity of CAR. (A) Structure of CAR and its neddylation inhibitory rate tested by AlphaScreen approach. (B) Survival curves and antiproliferation activities (IC_{50}) of CAR were analyzed by CCK8 assay, against human lung cancer cell lines A549 and H1299 for 72 h, respectively ($n = 3$). (C, D) Either A549 or H1299 cells were treated with CAR (10, 20 and 40 μmol/L) at indicated doses for 10 days to determine its therapeutic efficacy on clonogenic survival. 0.1% DMSO treated A549 cells as the control group. Checkboard test evaluated the synergistic effect of CAR combined with either ENT (E) or DOX (F) in A549 cells. A549 was treated with escalating doses of either ENT or DOX (0−100 nmol/L) on CAR (0−30 μmol/L) as indicated, followed by analysis of the cell proliferation rate; Percent inhibition of cell proliferation at each dose of drug is presented. (G−J) CAR inhibited A549 xenograft growth in nude mice ($n = 6$). After intraperitoneally administering vehicle, MLN4924 (30 mg/kg, qd), CAR (15 or 30 mg/kg, qd), ENT (10 mg/kg, qod) and the combination of CAR (15 mg/kg) and ENT (10 mg/kg, qod) for about four weeks (per five-days treatment with a two-day rest as the treatment cycle) until the tumor volume arrived to 1000 mm^3, the mice were sacrificed, and the tumors were weighed. Tumor volume changed during treatment (G); Body weight changed of mice during treatment (H); The tumorous weight of each group (I); The images of tumors from mice at 24 days after initiation of treatment (J). Statistical significance was determined by the Student's *t*-test (two-tailed): $^{**}P < 0.01$, $^{***}P < 0.001$, n.s. indicates no significant difference. Data are mean values ± SD ($n = 3$).

3.3. Target-focused preliminary SAR study clarifying the modification potential of the scaffold

Despite the bi-functional activities, the effective dose of CAR in anticancer therapy was higher than that of the cardioprotective therapy (30 mg/kg *vs* less than 10 mg/kg). Meanwhile, the neddylation inhibitory activity of CAR was weaker than its *β*-AR antagonistic activity. The unbalanced drawback of CAR might cause a potential side-effect or toxicity in the cardioprotective therapy at a high dose. By contrary, a low dose of CAR was insufficient to suppress the tumor growth. The results indicated that CAR is difficult to be utilized directly for the co-therapy of cancer and HF in clinic. In this study, chemical modification of CAR as a bi-functional leading compound, represented a reliable strategy to increase the anticancer effect and neddylation inhibitory activity, aiming to balance the interaction activities of "old" and "new" targets, along with their respective therapeutic efficacy.

Rational design of bi-functional drugs necessitates a comprehensive understanding of the structure−activity relationship (SAR) of repurposed drugs and their two distinct functions and targets. However, traditional drug discovery strategies, such as fragment-based, screen-based, and *de novo* drug discovery, face challenges in balancing the two functions or indications, due to ambiguous SARs of the bi-function interactive single or double

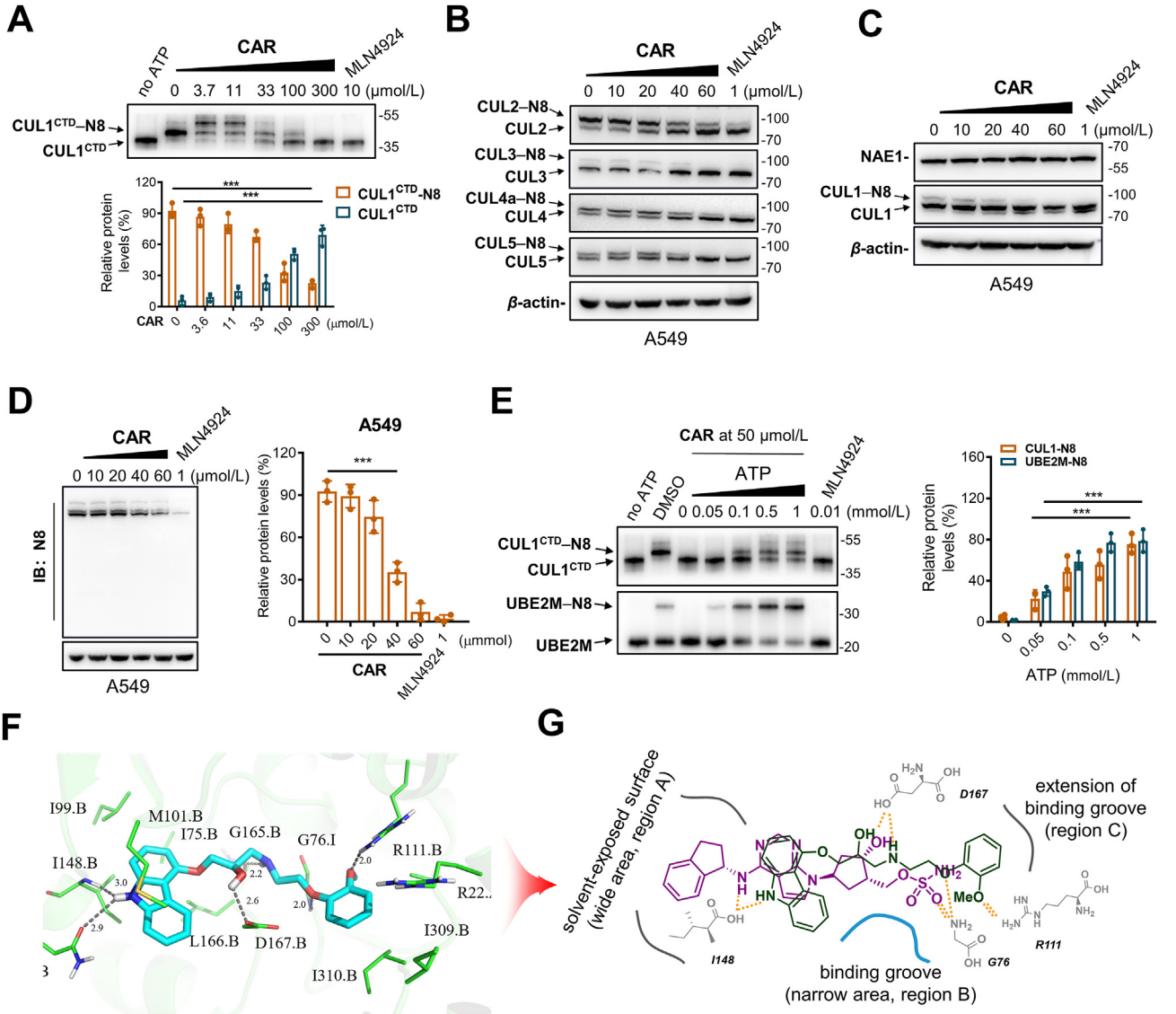

Figure 3 CAR might target NAE to inhibit the neddylation pathway. (A) Various concentrations of CAR inhibited the CUL1−Nedd8 adduct in the enzyme-based assay. (B) CAR blocked the cullins−Nedd8 pathway in A549 cells. (C) CAR decreased the CUL1−Nedd8 adduct without affecting the NAE1 level in A549 cells. (D) CAR inhibited the global Nedd8 modification in A549 cells. (E) CAR inhibited both CUL1−Nedd8 and UBE2M−Nedd8 formation with the addition of various concentrations of ATP in an enzyme-based assay. (F) Low-energy binding conformations of CAR (shown in blue) bound to NAE heterodimer generated by virtual ligand docking (PDB ID: 3GZN). The binding pocket of NAE was represented as a green ribbon form. Amino-acid residues and small molecules was depicted as a stick model showing carbon (green), hydrogen (white), oxygen (red), nitrogen (dark blue), and sulfur (yellow) atoms. H-bonds were indicated as the black lines. (G) Merging between top-ranked CAR pose (shown in green) and MLN4924 conformation (shown in purple) from NAE crystal (PDB ID: 3GZN). Amino-acid residues were shown in gray and H-bonds were indicated as the orange lines. 0.1% DMSO treated either protein solvent or cells as the control group. Statistical significance was determined by the Student's *t*-test (two-tailed): $^{***}P < 0.001$.

targets. Despite mature pharmacophore combination design, current multi-target drugs mainly focus on single-indication therapy, often with limited druggability. By contrary, target-focused repurposing adequately utilized the advantages offered by repurposed drugs, such as detailed information on structural evolution, clear interaction mechanism, SAR of the original target, and a rich commercial resource of homologue drugs, to gain insight into an initial but subtle SAR network of both original target and new target associated with the repurposed drug.

The present study initially dissected the scaffold of CAR into three moieties, including a carbazole head group, an oxy-1,2-propanolamine responsible for β-AR antagonistic activity, and a side chain comprising an ethoxyl linker chain and a catechol ether. Subsequently, a series of molecular docking studies were conducted to summarize the target-scaffold relationship of CAR binding to either β-AR or NAE as follows (Fig. 4, Supporting Information Fig. S8A and S8B), (i) both the NAE and β-AR binding pockets exhibited a similar spatial configuration, featuring a wide space with or without the solvent-exposed surface (region A), a narrow binding groove (region B), and a shallow extension of the binding groove (region C), (ii) CAR not only exhibited high affinity for the ATP-binding pocket of NAE, but also displayed a

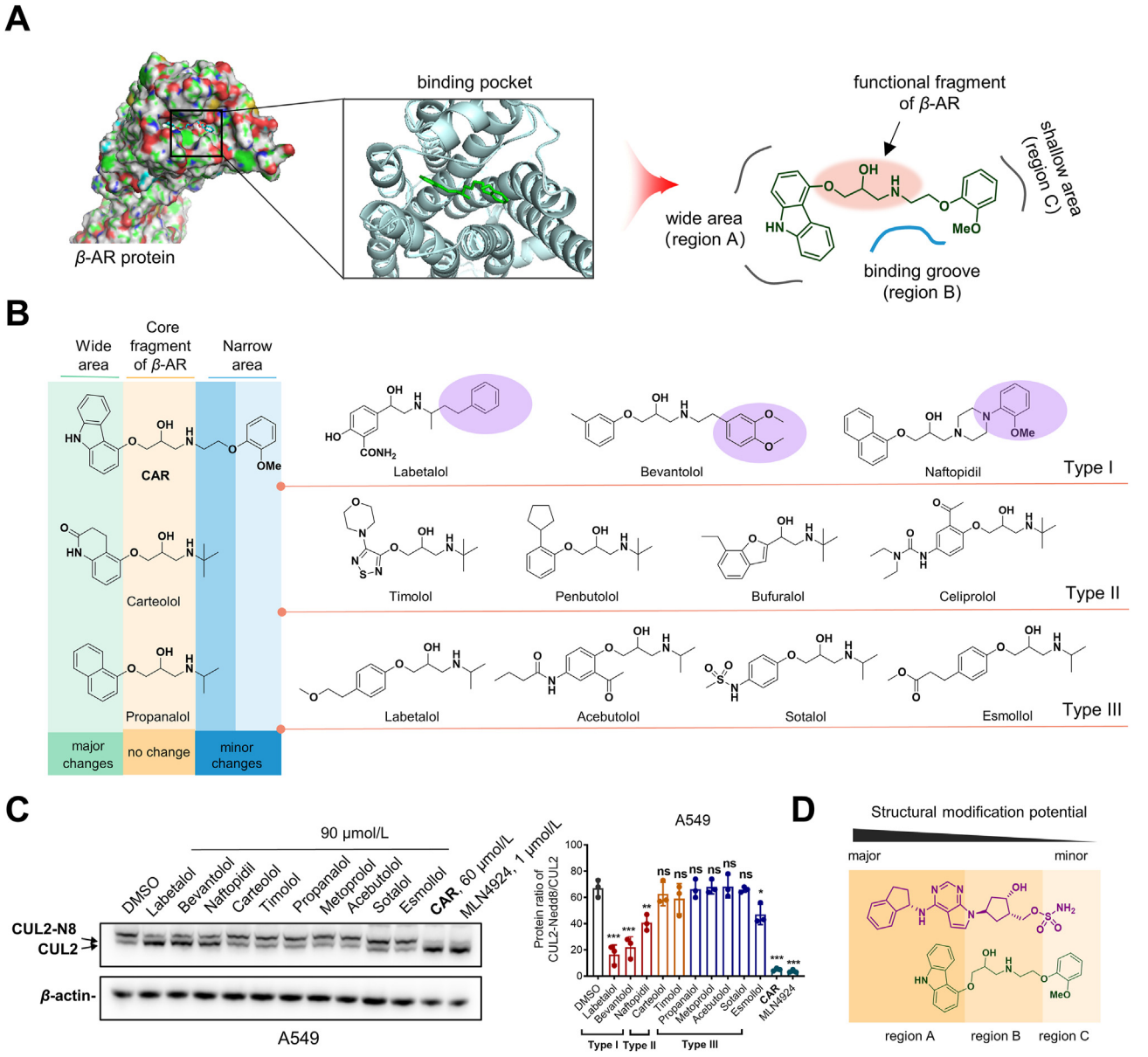

Figure 4 Preliminary SAR study of CAR. (A) Low-energy binding conformations of CAR (shown in green) bound to β-AR generated by virtual ligand docking (PDB ID: 6PS3). The binding pocket of β-AR was represented as a surface model showing carbon (green), hydrogen (white), oxygen (red), nitrogen (blue), and sulfur (yellow) atoms. (B) Types of β-AR antagonists were differentiated according to their structures, which corresponded to the potential binding attitude with the β-AR pocket. (C) Further evaluation of the CUL2−Nedd8 formation by the treatment of representative β-AR antagonists for 24 h in A549 cells. (D) Prediction of structure modification potential based on the primary SAR study. Statistical significance was determined by the Student's *t*-test (two-tailed): $*P < 0.05$, $**P < 0.01$, $***P < 0.001$, n.s. indicates no significant difference.

binding mode and multiple H-bonds similar to those of MLN4924, and (iii) the three moieties occupied corresponding regions in both binding pockets suggesting that the binding mode of CAR in NAE resembled that in β-AR.

Apart from CAR, β-AR antagonists with the "lol" suffix have been approved or entered clinical trials. Similar to CAR, these drugs possess scaffolds consisting of a head group with various aromatic substituents, a core oxy-1,2-propanolamine group, and a side chain. Based on differences in the side chain, we classified these drugs into three chemotypes (Fig. 4B). Type I "lol" drugs contained various linker chains with a catechol-like group, while type II and III drugs had *tert*-butyl and isopropyl side chains, respectively. We evaluated these three types of "lol" drugs for neddylation inhibition and found that only type I exhibited such activity (Fig. 4C). Combining these results with the target-scaffold studies of CAR, we summarized the initial SAR and modification potential of CAR as follows (Fig. 4D): (i) Only type I "lol" drugs displayed the neddylation inhibitory activities, indicating that the neddylation pathway was not directly regulated by β-AR. (ii) The high-tolerant region A provided an opportunity to enhance the neddylation inhibition while maintaining the β-AR antagonistic activity, through the introduction of various carbazole-like substituents. (iii) Regarding CAR specifically, its side

chain showed a preference for minor modifications due to its passage through a narrow binding groove in both the NAE and β-AR pockets. Moreover, the presence of catechol ether group in CAR was crucial for maintaining the neddylation inhibition and stability *in vivo*[27,31].

3.4. *Scaffold-driven derivative design and secondary SAR study*

Target-focused preliminary SAR study disclosed the similarity and difference of CAR binding to these two targets, and gave us new insight of CAR-based modification potential. In the context of scaffold-driven repurposed drug design, one major challenge is to enhance the off-target anticancer activity while maintaining the on-target cardioprotective activity of CAR, along with inheriting the original druggability. To this end, our derivative design strategy emphasized more about how to clearly and concisely identify the correlation between off-target and on-target activities with their associated scaffolds and pharmacophores (Fig. 5). Based on the preliminary SAR and the scaffold-driven drug repurposing approach, 44 CAR derivatives **1**−**44** were designed and synthesized in total (Supporting Information Schemes S1−S3)[32−34]. Further synthetic information can be found in the supporting information.

The present study first modified the binding sites of the *iso*-propanolamine moiety (derivatives **1**−**10**) (Fig. 5A; Table 1). Among them, enantiomers **1** and **2** had no significant difference in the anticancer activities and neddylation inhibitions compared to CAR. Methylation or acetylation of the hydroxyl and amido groups (derivatives **3**, **4**, and **5**, respectively) resulted in lower activities. By contrary, chloroacetylated **6** displayed better anti-proliferative activities than CAR, despite similar neddylation inhibitory activity. On the other hand, δ-lactams **7** and **8**, as well as their respective analogues **9** and **10**, whose *iso*-propanolamine moiety was cyclized, lost their activities against cancer cells. These finding indicated that the unmodified *iso*-propanolamine moiety was essential for maintaining the neddylation inhibition.

We then examined the SAR by replacing the ethoxyl linker chain with similar groups (Table 2). Removal of the ethoxyl group (derivative **11**) or conversion into various alkyl groups (derivatives **12**−**14**) led to a decrease in CUL1−Nedd8 inhibitory activities, while the antiproliferation effects of derivatives **12**−**14** were gradually increased with the chain length from one to three carbon atoms. The results suggested that the introduction of a lipophilic chain improved the antiproliferative effects of derivatives. Therefore, the propyl group of **14** was replaced with various vinyl groups (derivatives **15**−**17**) to further elevate the scaffold lipophilicity. Particularly, compound **15** with an unsubstituted allyl group showed better inhibitory activities than CAR. However, an additional propynol **18** showed slightly reduced potency. The replacement of the ethoxyl oxygen atom with nitrogenous groups (derivatives **19**−**22**) also resulted in a decrease in potency. Consequently, we selected **15** as a representative derivative for the next round of structural modifications.

Next, the critical carbazole moiety was evaluated for its effect on the balance of bi-functional activities (Fig. 5A and Table 3). We initially replaced the carbazole group of representative **15** with simple aromatic substituents originated from classical "lol" drugs (derivatives **23**−**26**). As expected, these derivatives scarcely increased the inhibitory activities. By contrary, the homologues **27**−**29**, in which the carbazole groups were substituted at the 2′, 3′, or 4′-position, respectively, displayed similar or improved neddylation inhibitory activities, compared to **15**. Particularly, the substitution at the 3′-position (derivative **28**) showed more potency than the other two positions, suggesting that the substituted positions of the carbazole ring also influenced the inhibitory activity. Then, several carbazole-like fused rings were introduced to replace the carbazole groups, including 4′ or 5′-position substituted indole groups (derivatives **30** and **31**), 1′ or 2′-position substituted naphthyl groups (derivatives **32** and **33**), 6′ or 7′-position substituted quinoline groups (derivatives **34** and **35**), and 5′ or 6′-position substituted quinolino groups (derivatives **36** and **37**). Among them, **30** and **31** retained the neddylation inhibitory activities, but exhibited lower antiproliferation effects, while **33** slightly improved the neddylation inhibition. However, derivatives **32** and **35**−**37** were devoid of inhibitory activities. Then, the scaffold hopping of representatives **28** and **33** provided the open cycle derivatives **38**−**44**. Concretely, the homologues **38**−**40** of **33** that replaced the naphthyl group with 2′, 3′, or 4′-position substituted biphenyl group, displayed better cellular neddylation and proliferation inhibitory activities. Particularly, the *para*-biphenyl **40** was superior to either *ortho*-biphenyl **38** or *meta*-biphenyl **39**. However, the replacement of the *para*-biphenyl group with the 4′-cyclohexyl phenyl group (**41**) resulted in a moderate loss of activities. In parallel, the homologues **42** and **43** of **28** that replaced the carbazole group with 3′ or 4′-position substituted diphenylamine, also displayed excellent potency, especially the 4′-diphenylamine **43**. However, the replacement of the 4′-diphenylamine group with the benzamide group (derivative **44**), led to a moderate loss of activities.

The secondary rounds of SARs are summarized as follows (Fig. 5B). (1) Oxy-1,2-propanolamine group served as a core bifunctional pharmacophore, and inappropriate modification might reduce the potency of derivatives. (2) Lipophilic side linker chains with a length of 3−5 carbon atoms contributed to improved inhibitory activities, with the allyl group being particularly favorable. (3) Regarding the aromatic head group, the suitable size of the substituent was crucial. Modifications in region A revealed that the potency increased in the order of substituted polyaryl > fused aryl > phenyl. Moreover, the substituted position also affected the potency, the *para*-position was the best-substituted position in the aromatic head group. Subsequently, the molecular docking study validated that representative **43** had nearly identical hydrogen-bonding interactions with MLN4924 in the NAE pocket (Fig. 5C). In addition, in comparison with CAR, **43** obviously displayed a more similar binding attitude to MLN4924, whose diphenylamine group almost overlapped the substituted adenosine of MLN4924 (Fig. 5C).

3.5. *Optimal **43** displayed potential bi-functional effects in cells*

Initially, a guinea pig atria test showed that representative derivatives **40** and **43** retained the β-AR antagonistic activities. Anthracyclines, such as doxorubicin (DOX), can induce myocardial cell injury and lead to LVD and HF[5] (Table 4). In this study, the DOX-induced rat myocardial cells H9c2 injury model was introduced to evaluate the cardioprotective effect of either derivative **40** or **43**. The results showed that these two treatment groups had higher cell viability rates than the control group, comparable with the CAR-positive group. The mechanism of DOX-associated cardiac injury involves the generation of reactive oxygen species (ROS). Previous studies also demonstrated that CAR displayed better anti-HF effect than other "lol" drugs, due to its additional antioxidant properties[35,36]. Therefore, a followed hypoxia/re-oxygenation (H/R)-induced cardiac injury assay was performed to simulate the DOX-induced cellular ROS injury to evaluate the cardioprotective activities of either **40** or **43**. Similarly, the two

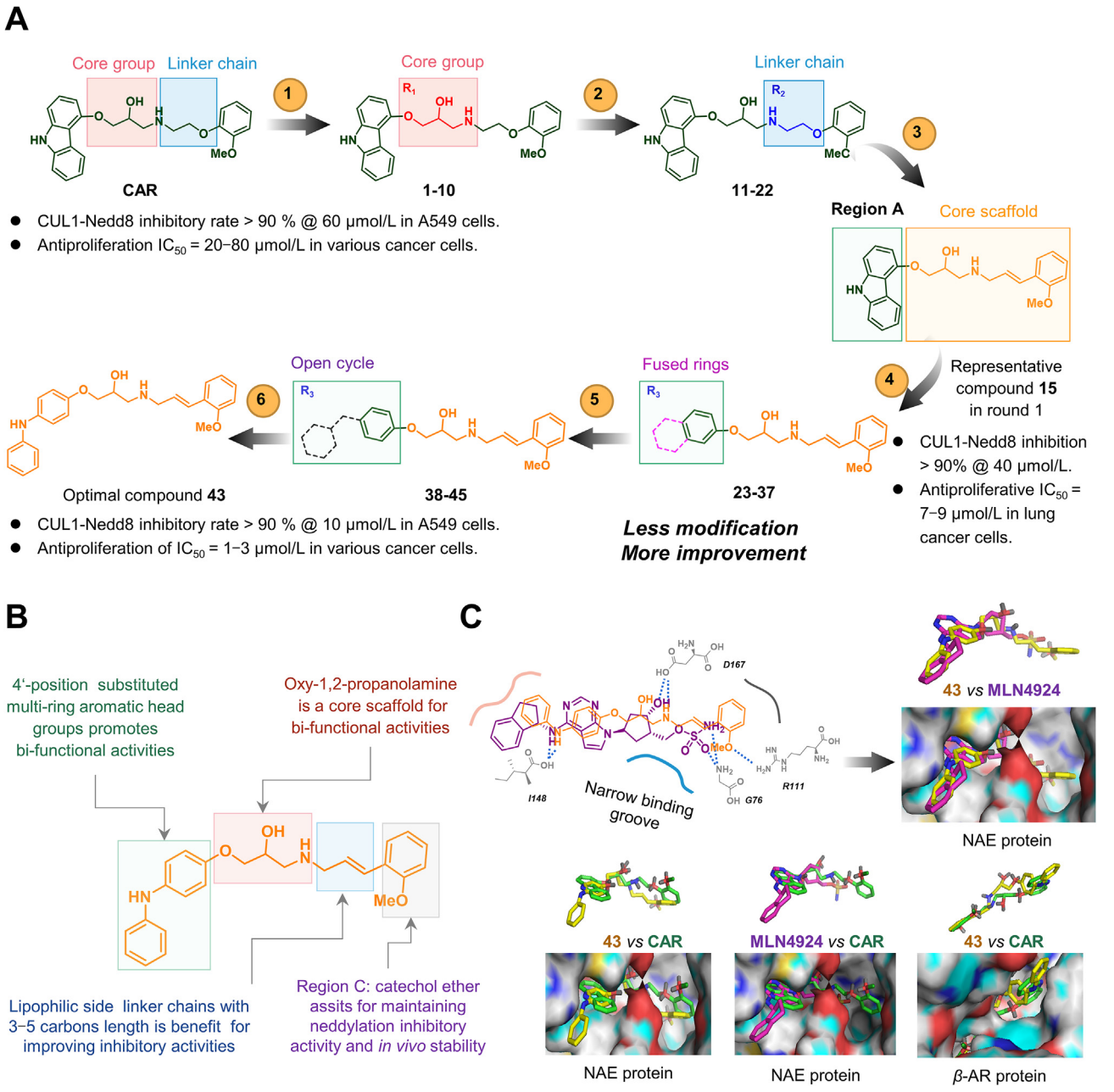

Figure 5 Optimal derivative **43** and secondary SAR study. (A) Scaffold-derived repurposing guided the structural evolution of lead compound CAR and increased the neddylation inhibitory and antitumor activities of CAR derivatives. (B) The secondary round of SAR study. (C) Merging the top-ranked pose of compound **43** (depicted in orange) with the conformation of MLN4924 (depicted in purple) from the NAE crystal structure (PDB ID: 3GZN) was performed. Amino acid residues are represented in gray, and H-bonds are depicted as blue lines. The binding conformation of compound **43** (depicted in yellow) and MLN4924 (depicted in purple) within the NAE pocket, as well as the binding conformation of compound **43** and CAR (depicted in green) within the NAE pocket, the binding conformation of MLN4924 and CAR within the NAE pocket, and the binding conformation of compound **43** and CAR within the *β*-AR pocket were analyzed.

treatment groups groups improved cell injury better than the control group. Alterations in cardiac energy metabolism are also a major adverse factor to HF[37]. An additional glucose deprivation was conducted to explore whether either **40** or **43** could overcome energy metabolism dysfunction induced cardiac injury. Interestingly, these two derivatives failed to attenuate the cellular damage progress. To evaluate their capacity against the neddylation-activated cell lines, we tested the seven cancer cell lines using the CCK-8 assay, which included two human lung cancer cell lines A549 and H1299, two human breast cancer cell lines T-47D and MB231, two human liver cancer cell lines HepG2 and Huh7, and one human colon cancer cell line SW480 (Table 4). In general, either **40** or **43** inhibited the cancer cell growth at the single digit micromolar level. However, a preliminary *in vivo* survival experiment showed that compound **40** displayed potential toxicity at the dose of 20 mg/kg, compared to compound **43** (Supporting Information Fig. S9). Considering the druggable potential, we chose **43** for further evaluation in this study.

Table 1 Chemical structures of derivatives **1**−**10** and their CUL1−Nedd8 inhibitory activities in A549 cells and antiproliferative activities in A549 and H1299 cell lines.

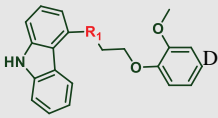

Derivatives **1**−**10**

Compd.	R_1	Antiproliferation (A549/H1299, IC_{50}, μmol/L)	CUL1−Nedd8 inhibitory rate[a]	Compd.	R_1	Antiproliferation (A549/H1299, IC_{50}, μmol/L)	CUL1−Nedd8 inhibitory rate[a]
1	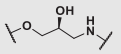	23.4/41.5	67% @ 40 μmol/L (60 μmol/L)[b]	**7**	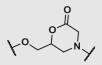	13.4/>100	>80 μmol/L
2	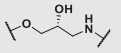	34.2/50.2	64% @ 40 μmol/L (60 μmol/L)[b]	**8**	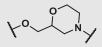	>100/>100	>80 μmol/L
3	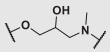	33.3/39.5	>80 μmol/L	**9**	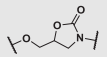	>100/>100	>80 μmol/L
4	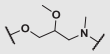	78.5/>100	>80 μmol/L	**10**		>100/>100	>80 μmol/L
5	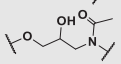	37.1/88.5	55% @ 80 μmol/L	CAR		22.9/44.7	73% @ 40 μmol/L (60 μmol/L)[b]
6	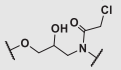	13.8/4.2	>10% @ 40 μmol/L (60 μmol/L)[b]	MLN		0.8/0.9	1 μmol/L[b]

[a]The CUL1−Nedd8 inhibitory rate of compounds was explored at the concentrations of 40, 60, and 80 μmol/L in turns, respectively.
[b]The CUL1−Nedd8 inhibitory rate over 90% at the concentration.

Table 2 Chemical structures of derivatives **11**−**22** and their CUL1−Nedd8 inhibitory activities in A549 cells and antiproliferative activities in A549 and H1299 cell lines.

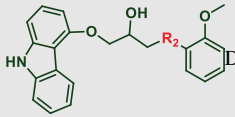

Derivatives **11**−**22**

Compd.	R_2	Antiproliferation (A549/H1299, IC_{50}, μmol/L)	CUL1−Nedd8 inhibitory rate[a]	Compd.	R_2	Antiproliferation (A549/H1299, IC_{50}, μmol/L)	CUL1−Nedd8 inhibitory rate[a]
11		86.8/>100	>60 μmol/L	**18**	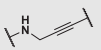	>100/>100	>60 μmol/L
12		13.9/14.8	52% @ 60 μmol/L	**19**	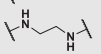	6.4/9.0	>10% @ 20 μmol/L (40 μmol/L)[b]
13		13.3/15.2	>10% @ 40 μmol/L (60 μmol/L)[b]	**20**	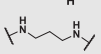	10.8/8.9	>10% @ 20 μmol/L (40 μmol/L)[b]
14		11.8/7.2	>10% @ 40 μmol/L (60 μmol/L)[b]	**21**	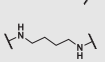	15.4/10.6	>10% @ 40 μmol/L (60 μmol/L)[b]
15		7.9/7.2	55% @ 20 μmol/L (40 μmol/L)[b]	**22**		>100/>100	>60 μmol/L
16		8.5/8.9	36% @ 20 μmol/L (40 μmol/L)[b]	CAR		22.9/44.7	73% @ 40 μmol/L (60 μmol/L)[b]
17	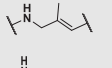	9.7/8.7	>10% @ 20 μmol/L (40 μmol/L)[b]	MLN		0.8/0.9	1 μmol/L[b]

[a]The CUL1−Nedd8 inhibitory rate of compounds was explored at the concentrations of 20, 40, and 60 μmol/L in turns, respectively.
[b]The CUL1−Nedd8 inhibitory rate over 90% at the concentration.

Table 3 Chemical structures of derivatives **23**–**44** and their CUL1–Nedd8 inhibitory activities in A549 cells and antiproliferative activities in A549 and H1299 cell lines.

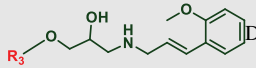

Derivatives **23**–**44**

Compd.	R_3	Antiproliferation (A549/H1299, IC_{50}, μmol/L)	CUL1–Nedd8 inhibitory rate[a]	Compd.	R_3	Antiproliferation (A549/H1299, IC_{50}, μmol/L)	CUL1–Nedd8 inhibitory rate[a]
23		17.4/33.1	>40 μmol/L	**35**		44.3/>100	>40 μmol/L
24		>100/34.1	>40 μmol/L	**36**	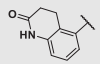	>100/>100	>40 μmol/L
25		>100/>100	>40 μmol/L	**37**		>100/>100	>40 μmol/L
26		31.6/11.4	>40 μmol/L	**38**		2.1/3.6	31% @ 5 μmol/L (10 μmol/L)[b]
27		6.8/3.9	62% @ 20 μmol/L (40 μmol/L)[b]	**39**	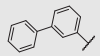	4.2/4.8	44% @ 5 μmol/L (10 μmol/L)[b]
28		9.1/6.1	41% @ 10 μmol/L (20 μmol/L)[b]	**40**	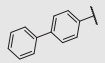	3.1/2.4	51% @ 5 μmol/L (10 μmol/L)[b]
29		11.2/16.3	34% @ 20 μmol/L (40 μmol/L)[b]	**41**	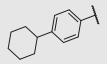	11.2/29.5	>40 μmol/L
30		26.9/23.1	>10% @ 20 μmol/L (40 μmol/L)[b]	**42**	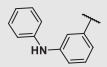	2.7/3.5	61% @ 10 μmol/L (20 μmol/L)[b]
31		25.4/25.3	>10% @ 20 μmol/L (40 μmol/L)[b]	**43**	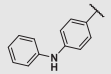	1.3/2.4	43% @ 5 μmol/L (10 μmol/L)[b]
32		16.9/19.8	>40 μmol/L	**44**	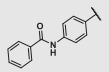	3.3/3.9	55% @ 20 μmol/L (40 μmol/L)[b]
33		17.1/16.3	33% @ 20 μmol/L (40 μmol/L)[b]	CAR		22.9/44.7	73% @ 40 μmol/L (60 μmol/L)[b]
34		28.1/36.6	>40 μmol/L	MLN		0.8/0.9	1 μmol/L[b]

[a]The CUL1–Nedd8 inhibitory rate of compounds was explored at the concentrations of 5, 10, 20, and 40 μmol/L in turns, respectively.
[b]The CUL1–Nedd8 inhibitory rate over 90% at the concentration.

Table 4 Evaluation of representative **40** and **43** on the β-AR antagonistic activities, the cardioprotective efficacy of H9c2 cells by DOX injury model, H/R injury model and GD injury model, the antiproliferation activities of multiple cancer cell lines.

Compd.	β-AR antagonistic activity (IC_{50}, μmol/L)	H9c2 viability rate, % @ 1 μmol/L			Lung cancer cell lines (IC_{50}, μmol/L)		Breast cancer cell lines (IC_{50}, μmol/L)		Liver cancer cell lines (IC_{50}, μmol/L)		Colon cancer cell line SW480 (IC_{50}, μmol/L)
		DOX injury model	H/R injury model	GD injury model	A549	H1299	T-47D	MB231	HepG2	Huh7	
40	0.09	62.6%	41.7%	58.2%	1.2 ± 0.4	3.0 ± 0.7	1.9 ± 0.1	1.2 ± 0.2	1.7 ± 0.2	3.5 ± 0.3	2.7 ± 0.1
43	0.17	61.8%	42.0%	51.5%	0.8 ± 0.3	3.2 ± 0.7	2.6 ± 0.2	1.1 ± 0.2	3.0 ± 1.1	3.9 ± 1.1	2.9 ± 0.3
CAR	0.06	57.2%	41.3%	57.7%							
Empagliflozin				71.6%							
DMSO		49.1%	31.3%	57.2%							

Having confirmed the CUL1−Nedd8 and multiple cancer cell proliferation inhibitory activities, we further evaluated the targeted inhibitory effect of representative **43** with a dose-dependent assay in cancer cell lines A549 and H1299. The results showed that **43** not only completely inhibited the levels of CULs−Nedd8 adducts without affecting the NAE1 level (Fig. 6A, B; and Supporting Information S10A), but also eliminated the global Nedd8 modification (Fig. 6C). Furthermore, ubiquitination is a highly homologous pathway with neddylation. To explore the inhibitory activity of ubiquitination is a general approach to evaluate the selectivity of neddylation inhibitors[23]. Western blotting assay showed that compound **43** have no significant inhibitory activity on ubiquitination, suggesting it selectivity in inhibiting the neddylation pathway (Fig. S10B). Moreover, **43** suppressed the clonogenic survival of A549 and H1299 cells at the low concentration (Fig. 6D). An additional annexin-V/PI double staining assay indicated that **43** induced the apoptosis of A549 and H1299 cells (Fig. 6E−H). In addition, we also synthesized the chiral **43**, (*R*)-**43** and (*S*)-**43**, and then evaluated their neddylation inhibitory and anti-proliferation activities. The results showed that (*R*)-**43** seemingly displayed no significant difference with (*S*)-**43** in A549 cells (Supporting Information Fig. S11).

*3.6. Compound **43** suppresses the growth of A549 xenograft tumors in mice*

Inspired by the impressive *in vitro* activities, we further investigated the potential antitumor effects of compound **43** *in vivo*. In the initial approach, mice were bearing A549 cancer cells to investigate the maximum tolerated doses and anticancer efficacy of **43** and DOX, respectively (Supporting Information Fig. S12). The results showed that all mice of the DOX-treated group and one mouse of the CAR-treated group with the dose of 30 mg/kg were dead within 20 days, respectively (Fig. S12A and S12B). Two **43**-treated groups exhibited superior tumor growth inhibition than CAR, without the mice weight loss (Fig. S12C and S12D).

Based on the preliminary dose investigation, **43** further evaluated the potential of the other A549 xenograft model with the adjusted doses of regimens (Fig. 7A). In contrast to the control group, all treatment groups significantly decreased tumor volume and tumor weight after 30 days (Fig. 7B, D, and E). Furthermore, **43** displayed the dose-dependent activities in combination with the results of the preliminary dose investigation. Herein, **43**-treated group with the dose of 5 mg/kg showed higher tumor growth inhibition percentage (TGI) than DOX-treated group with the dose of 2 mg/kg (50.5% *vs* 34.5%), comparable with CAR-treated group with the dose of 30 mg/kg (44.5%). Compared with either control or CAR groups, **43**-treated groups with the dose of either 20 or 5 mg/kg barely affected the body weight (Fig. 7C).

*3.7. Compound **43** displays cardioprotective efficacy of DOX-induced HF in C57 mice*

Our preliminary dose investigation validated that the mice HF were induced by the treatment of 1−5 mg/kg doses of DOX. In this study, the adjusted dose of DOX was pre-treated alone for three weeks to induce the C57 mice HF and then treated with either **43** (10 mg/kg, qd) or CAR (10 mg/kg, qd) for another three weeks (Fig. 8A). The results showed that either **43** or CAR decelerated the mice's weight loss caused by DOX (Fig. 8B). The

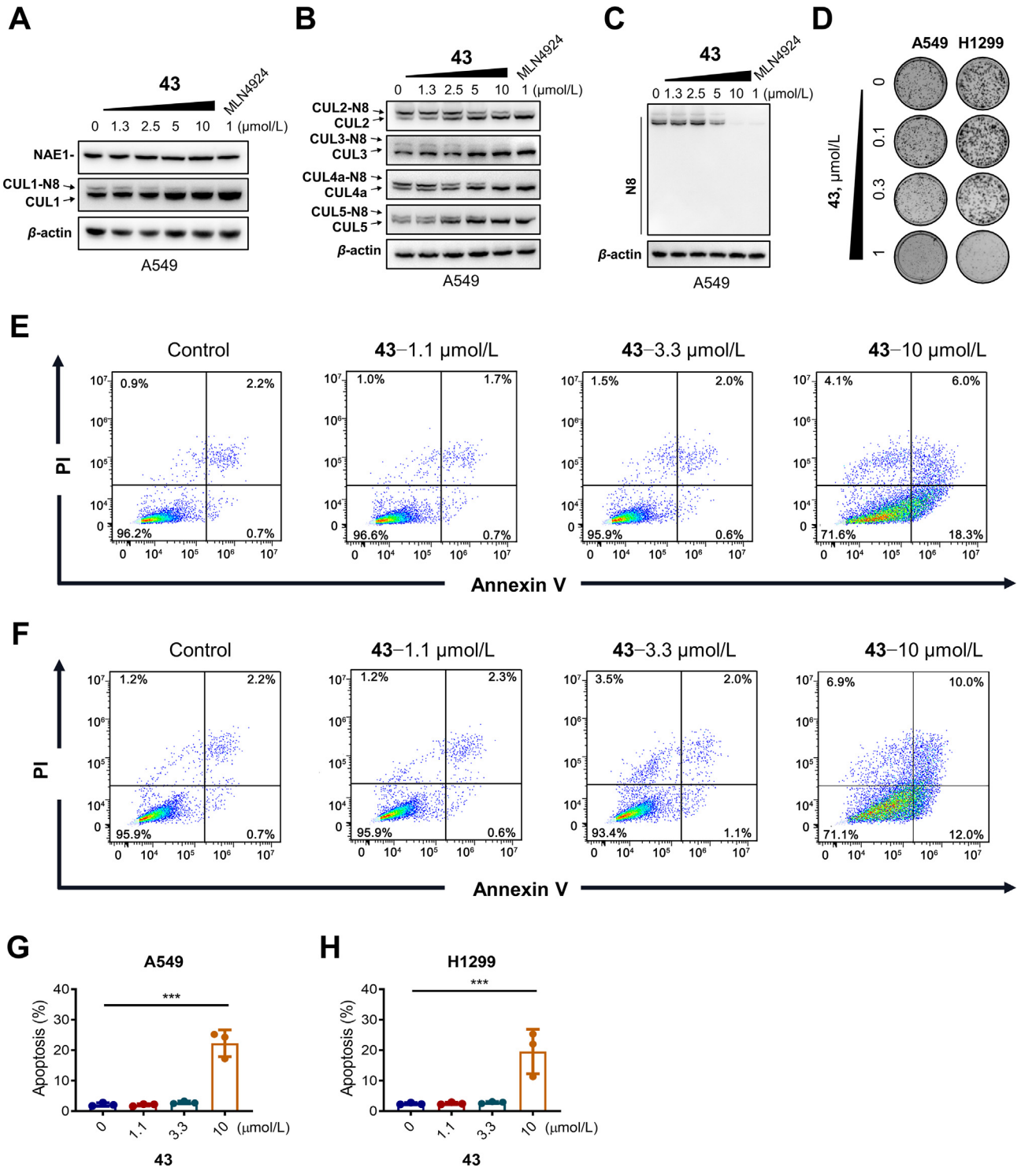

Figure 6 Compound **43** presented promising neddylation inhibitory activity and anticancer effect. (A) **43** decreased the CUL1−Nedd8 adduct in A549 cells. (B) **43** blocked the cullins−Nedd8 pathway in A549 cells. (C) **43** inhibited the global Nedd8 modification in A549 cells. (D) Either A549 or H1299 cells were treated with **43** (0.1, 0.3, and 1 μmol/L) at indicated doses for 10 days to determine its therapeutic efficacy on clonogenic survival. 0.1% DMSO treated A549 cells as the control group. (E−H) Evaluation of apoptosis on either A549 (E, G) and H1299 (F, H) cells by the treatment of with **43** (1.1, 3.3, and 10 μmol/L) for 72 h by Annexin V/PI staining and flow cytometry detecting. 0.1% DMSO treated A549 cells as the control group. $*P < 0.05$, $**P < 0.01$, $***P < 0.001$, n.s. indicates no significant difference.

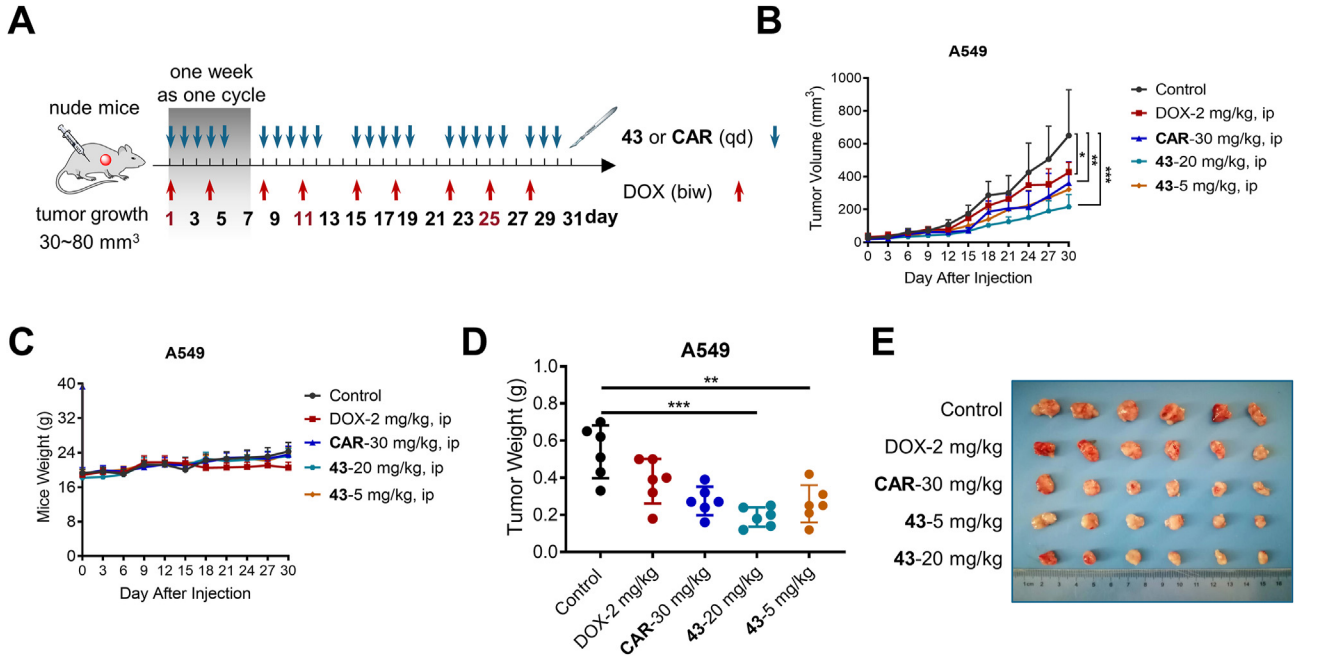

Figure 7 Compound **43** inhibited A549 xenograft growth in nude mice ($n = 6$). (A) Schematic representation of administration on A549 bearing mice. Five different regimens, including control group (saline), DOX treatment (2 mg/kg) as one positive group, CAR treatment (30 mg/kg) as the other positive group, two **43**-treated groups (5 or 20 mg/kg), were performed with an intraperitoneally administering for five days with a two-day rest as the treatment cycle. (B) Tumor volume changed during treatment; (C) Body weight changed of mice during treatment. (D) The tumorous weight of each group. (E) The images of tumors from mice at 31 days after initiation of treatment. Statistical significance was determined by the Student's *t*-test (two-tailed): $^{*}P < 0.05$, $^{**}P < 0.01$, $^{***}P < 0.001$.

M-mode echocardiograms showed that **43** markedly ameliorated left ventricular systolic dysfunction (LVSD) induced by DOX, comparable to CAR (Fig. 8C). The left ventricular end-diastolic diameter (LVDd) and end-systolic diameter (LVDs) of **43** and CAR-treated groups decreased (Fig. 8D, E), while their left ventricular ejection fraction (LVEF) and fractional shortening (LVFS) increased (Fig. 8F, G). In addition, two classical HF-associated myocardial enzymes were investigated in this study, including creatine kinase-MB (CK-MB), lactic dehydrogenase (LDH) (Supporting Information Fig. S13A and S13B). Unexpectedly, despite the increase of these two markers in the single DOX-treated group, the combination of either CAR or **43** failed to re-suppress the accumulation of CK-MB and LDH. Hence, the echocardiography had emerged as a major approach for our followed *in vivo* cardioprotection evaluation.

*3.8. Compound **43** displayed bi-functional effects in A549-bearing DOX-induced HF nude mice models*

In this study, we first established an A549-bearing DOX-induced HF nude mice model to systematically evaluate the anticancer and potential cardioprotective activities of **43**. Based on the dose-efficacy results above, seven regimens with a decreasing frequency of administration, for six days with a one-day rest as the treatment cycle (Fig. 9A). Among them, combination groups were set to simulate the supportive administration during the chemotherapy intermission. Overall, all **43**-treated groups showed better anticancer effects than the DOX treatment group, while having no significant effect on the body weight of the mice (Fig. 9B–E). Meanwhile, all treatment groups displayed no significant change of organ/body rate (Fig. 9F). Notably, the **43**-treated group by oral administration presented significant tumor inhibitory activity, comparable with the DOX-treated group. In addition, the combination-treated group displayed similar efficacy with single **43**-treated groups, suggesting that the combination strategy scarcely interfered with the anticancer efficacy of either **43** or DOX. HE staining of mice hearts showed that the DOX-treated group led to significant deteriorate phenotype, such as myocardial fiber disorder, myocardial edema and degeneration, compared to control group. On the contrary, the combination of **43** could alleviate the deterioration induced by DOX (Supporting Information Fig. S14A). Ki67 staining assay of tumors showed that compound **43** suppressed the tumor growth (Fig. S14A and S14B). Furthermore, HF always leads to a loss or significant decrease in movement functions of cancer survivors. In this study, both the rotarod and grip strength tests were conducted to evaluate the movement function of mice that were trained continuously for five days (Fig. 9G, H). In contrast with normal mice, the single DOX-treated group showed a clear motor decline, while the two combination-treated groups significantly recovered the decline movement induced by DOX. Notably, the single DOX-treated group occurred the mice death at the later stage of movement evaluations (Fig. S14C), suggesting the serious adverse effects of DOX in the life qualify. Despite having no influence for anticancer and movement evaluations, the following cardioprotection evaluation had to be terminated, due to a lack of enough samples of the single DOX-treated group. Collectively, the results validated that **43** displayed significant bi-functional efficacy to suppress the tumor growth and rescue the HF-induced movement decrease.

After confirming the bi-functional activities, we further evaluated the supportive ability of **43** with a lower frequency of administration on the advanced A549-bearing and lower dose DOX-induced HF

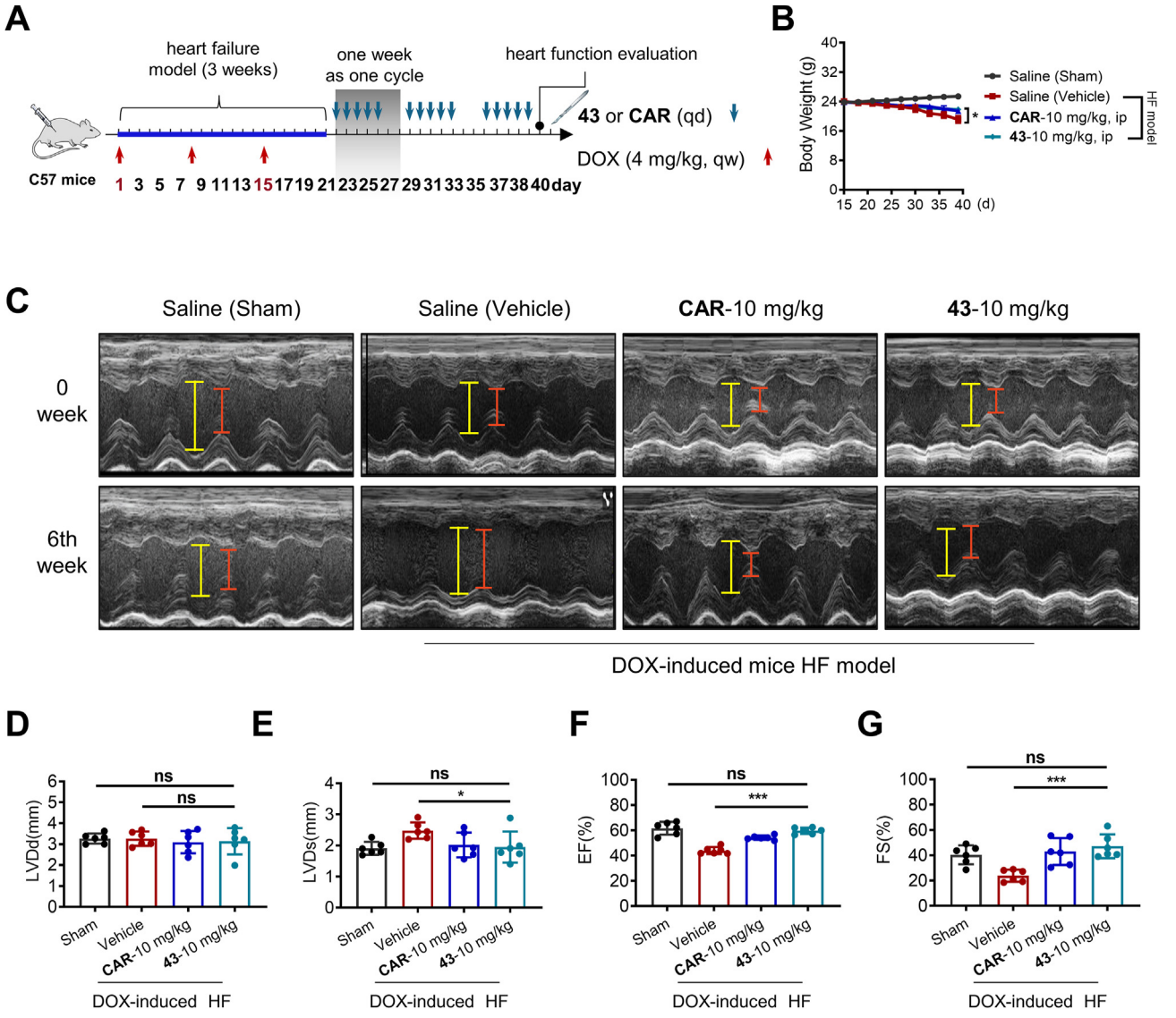

Figure 8 Compound **43** improved the LVD of DOX-induced HF C57 mice ($n = 6$). (A) Schematic representation of administration on DOX-induced HF C57 mice model. Four different regimens, including the sham group (saline), DOX-induced HF group as vehicle (saline), DOX-induced HF group with the treatment of CAR as the positive group, DOX-induced HF group with the treatment of **43**. Herein, DOX-induced HF groups were treated with DOX (4 mg/kg) in advance for three weeks, qw, then were performed with an intraperitoneally administration of saline, CAR (10 mg/kg) or **43** (10 mg/kg), for five days with a two-day rest as the treatment cycle, respectively. (B) Body weight changed of mice during treatment. (C) M-mode images of the left ventricle by using an echocardiographic scanner, the distances of LVDd (yellow lines) and LVDs (red lines). (D−G) Heart functional tests. Statistical significance was determined by the Student's *t*-test (two-tailed): $^{*}P < 0.05$, $^{***}P < 0.001$, n.s. indicates no significant difference.

nude mice, which simulated the real situation of chemotherapy and supportive treatment. Four regimens were applied with a metronomic schedule, for five days with a two-day rest as the treatment cycle (Fig. 10A). Once tumors reached an average volume of ~200 mm^3, mice were alternately treated with DOX or **43** in combination for 21 days to evaluate the anticancer activities. Then, these mice performed interval training for another week to evaluate the cardioprotective efficacy and movement functions. The results showed that the LVEF, LVFS, left ventricular posterior end-diastolic wall thickness (LVPWd), and left ventricular posterior end-systolic wall thickness (LVPWs) of the combination-treated group were increased, while the LVDd and LVDs decreased, compared with those of control group (Fig. 10B−G; and Supporting Information Fig. S15A). Despite no significant differences on mice organ and weight (Fig. 10I, L), the DOX-treated group led to both the heart deterioration and the motor decline, compared to the control group (Fig. 10H and Fig. S15B). By contrary, the combination-treated group significantly alleviated the heart deterioration and blocked the motor decline induced by DOX. Interestingly, the combination group also displayed a slight synergistic anticancer effect in the advanced A549 bearing DOX-induced HF nude mice (Fig. 10J−M). In addition, the pharmacokinetic analysis of injectable administration revealed that **43** had a C_{max} of 318 ng/mL and a half-life ($t_{1/2}$) of 7.9 h (Supporting Information Table S2). Collectively, derivative **43** represented an ideal supportive agent to be treated in the intermission of chemotherapy.

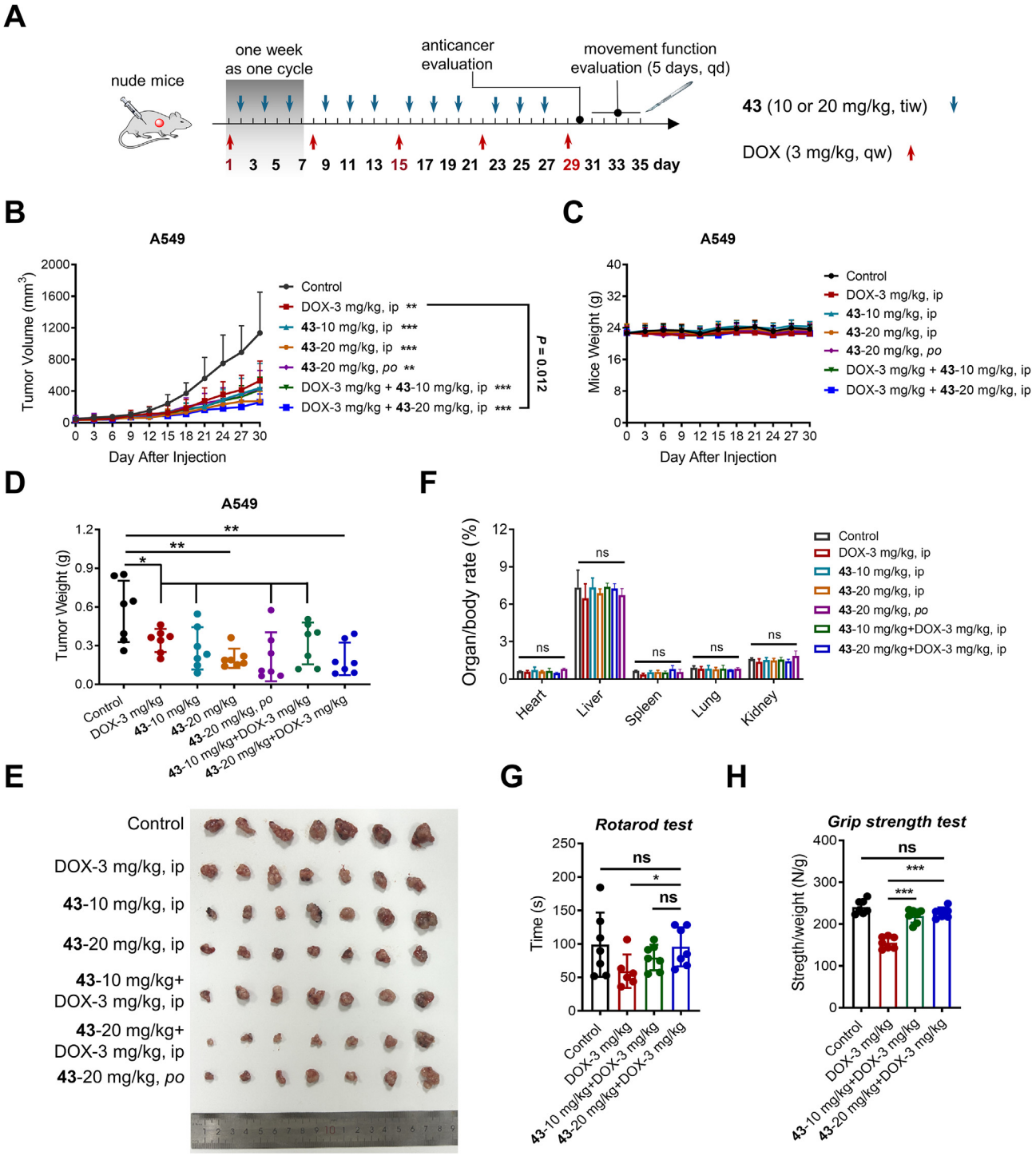

Figure 9 Compound **43** suppressed the tumor growth and improved the movement function of A549 bearing DOX-induced HF nude mice ($n = 7$). (A) Schematic representation of administration on the A549 bearing DOX-induced HF nude mice model. Seven different regimens, including the control group, DOX-treated group (3 mg/kg, ip), three single **43**-treated groups (10 and 20 mg/kg, ip; 20 mg/kg, *po*), and two combination-treated groups (DOX + **43**) with the same administration as the single treatment ones that were performed with a metronomic schedule, for six days with a one-day rest as the treatment cycle. Then, these mice were trained for five days (qd) to evaluate the movement functions. (B) Tumor volume changed during treatment. (C) Body weight changed of mice during treatment. (D) The tumorous weight of each group. (E) Images of tumors from mice after completing mice movement training. (F) Organ/body weight rate after 35 days of initial treatment. (G) Quantification of maximal time in rotarod from mice in the representative groups. (H) Quantification of the ratio of grip strength to weight from mice in the representative groups. Statistical significance was determined by the Student's *t*-test (two-tailed): $^{*}P < 0.05$, $^{**}P < 0.01$, $^{***}P < 0.001$, n.s. indicates no significant difference.

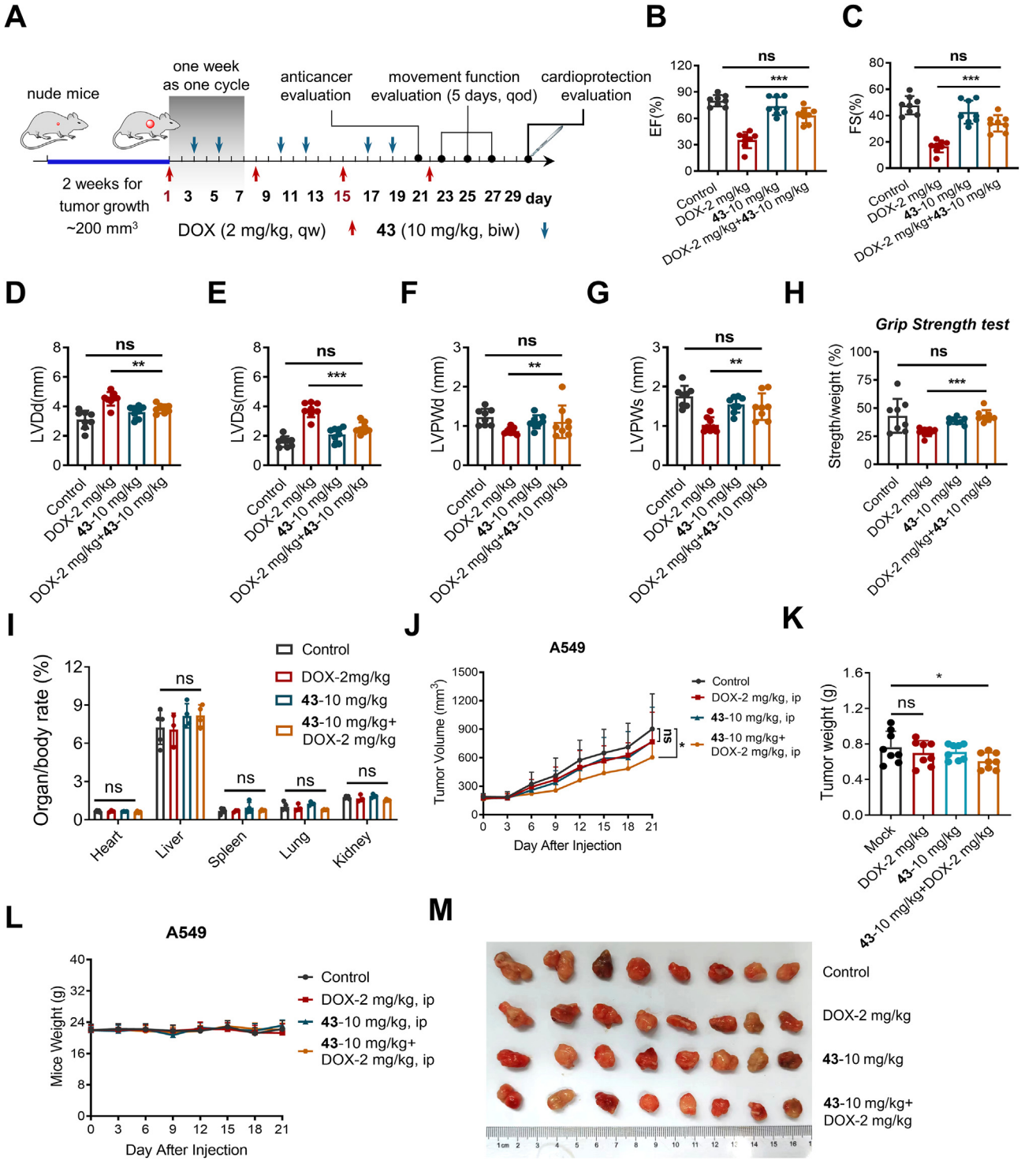

Figure 10 Compound **43** improved the LVD of advanced A549 bearing DOX-induced HF nude mice ($n = 8$). (A) Schematic representation of administration on A549 bearing DOX-induced HF nude mice model. Four regimens were applied, including control group, DOX-treated group (2 mg/kg, ip), the single **43**-treated group (10 mg/kg, ip), and the combination-treated group (DOX + **43**) with the same doses as the single treatment ones that were performed with a metronomic schedule, for five days with a two-day rest as the treatment cycle. Once tumors reached an average volume of ~200 mm^3, mice were alternately treated with DOX or **43** in combination for 21 days to evaluate the anticancer activities. Then, these mice were trained for five days (qod) to evaluate the movement functions and cardioprotective efficacy. (B−G) Heart functional tests. (H) Quantification of the ratio of grip strength to weight from mice in different groups. (I) Organ/body weight rate after 30 days of initial treatment. (J) Tumor volume changed during treatment. (K) The tumorous weight of each group. (L) Body weight changed of mice during treatment. (M) Images of mice tumors from mice after completing mice heart function evaluation. Statistical significance was determined by the Student's *t*-test (two-tailed): $^{*}P < 0.05$, $^{**}P < 0.01$, $^{***}P < 0.001$, n.s. indicates no significant difference.

4. Conclusions

Nowadays, drug repurposing has contributed to a variety of disease therapies, such as oncology, cardiovascular diseases, neurodegenerative diseases, infectious diseases, and metabolic disorders. One significant advantage of drug repurposing over traditional drug discovery is that repurposed drugs possess well-characterized pharmacology and safety profiles, thus reducing the risk of adverse effects in the preclinical and clinical phases. As advocated by Nobel Prize-winning pharmacologist James Black that "the most fruitful basis of the discovery of a new drug is to start with an old drug"[38]. Our previous studies had repurposed several drugs in various domains, such as repurposing of antifungal naftifine for antibacterial therapy[39], the antihypertensive candesartan cilexetil for anticancer therapy[40,41], and antialcoholic disulfiram for the antidiabetic therapy[42]. However, these studies mainly utilized the repurposed drugs as a conventional lead compound to conduct a traditional drug design, with little emphasis on the application of their unique advantages, including potential non-pharmacological characteristics, unambiguous on-target functions/activities and their interaction mechanisms, clear structural evolution and on-target SAR, and abundant derivatives and homologues for conveniently exploring the off-target SAR. Dependent on these advantages, the present study thus proposed a novel concept of the "trilogy of drug repurposing" to verify a new and important application of the old drug in disease and its complication co-therapies.

HF is a severe late complication of cancer survivors with a poor prognosis and limited treatment options, which can be caused or exacerbated by multiple diseases and treatment-related factors. Chemotherapy-induced HF is one of the most common issues among patients with advanced cancers. Despite recognizing the risks associated with chemotherapy, it remains challenging to replace it in developing countries due to its low cost, accessibility, and acceptable clinical outcomes. Data projections predicted that up to 4.2 million new patients in China will meet the criteria for chemotherapy in 2040, accounting for 27.8% of global chemotherapy needs[43]. The life-threatening complications induced by chemotherapy encompass various diseases, including neutropenia, neuropathy, organ dysfunction, and damage. Despite receiving increased attention for complication management, the reliable approaches have limitations, along with additionally compromised treatment outcomes and excess healthcare costs. Therefore, it is necessary for medicinal researchers to explore a feasible drug discovery strategy, aiming to supplement and assist the management and therapy of chemotherapy-induced complications.

In this study, we conceptualized the "trilogy of repurposing" strategy in developing a bi-functional agent. The proof of concept was initiated by screening the 193 approved cardiovascular drugs to investigate their additional anticancer functions. β-Blocker CAR which is commonly used in clinical cardioprotection, was demonstrated to suppress the lung cancer growth. Moreover, we also investigated that CAR might target protein NAE to inhibit the overactive neddylation pathway as a potential anticancer mechanism. After validating the new anticancer function, we further addressed the unbalanced drawback of CAR in anticancer and cardioprotection therapies. Through target-focused drug repurposing, we integrated the bi-functional activity relationships of CAR with targets NAE and β-AR, summarizing the preliminary SAR study. Guided by the SAR preliminary study, we proposed the strategy of scaffold-driven drug repurposing to balance the bi-functional activities. Forty-four CAR derivatives were designed and synthesized under the requirements of this strategy, to evaluate the neddylation and anticancer inhibitory activities. Finally, derivative **43** was carefully selected since it exhibited favorable characteristics *in vitro*, including multiple cancer cell antiproliferation activities (IC_{50} = 1−3 μmol/L), compelling neddylation inhibitory activity (CUL1−Nedd8 inhibitory rate >90 % @ 10 μmol/L), and β-AR antagonistic activities (IC_{50} = 0.17 μmol/L). Moreover, **43** displayed promising cardioprotective activity in both DOX-induced and H/R-induced cardiac injury models. Significantly, this study established several novels *in vivo* evaluation models, such as tumor-bearing DOX-induced mice models, which adequately demonstrated the bi-functional activities of derivatives **43**. Consequently, the favorably supportive ability of **43**, combined with its promising draggable profiles, suggested that the "trilogy of repurposing" strategy meets the requirement of cancer and its complication co-therapies.

We also believe that the "trilogy of repurposing" strategy may meet the requirement of artificial intelligence (AI)-based drug discovery and development (DDD). In recent years, AI-based DDD, combined with machine learning (ML), and deep learning (DL) approaches, is extensively applied in big data analysis, virtual screening, *de novo* drug design, and more. Undoubtedly, drug repurposing stands in the center of AI-based DDD, and nearly all success stories of AI-based DDD were related to drug repurposing. We speculated that the huge, objective, immutable, and cross-verifiable parameters and clinical information of old drugs provide AI with a logical framework for empowering drug discovery. However, the current AI-based DDD still falls short in evolving a rational development pathway for repurposed drugs, as it largely inherits the traditional drug design logic. By contrary, the present study adequately showed the difference of traditional drug design and repurposed drug re-designing during the process of "trilogy of drug repurposing". We believed that this strategy offers a potential logic for repurposed drug re-designing in AI-based DDD, especially in the development of co-therapy drugs.

Acknowledgments

This work was supported by the National Natural Science Foundation of China (Grant Nos. 22177076, 81820108022, 22037002), the Shanghai Frontier Science Center of Optogenetic Techniques for Cell Metabolism (2021 Sci & Tech 03-28, China), Shanghai Frontiers Science Center of Disease and Syndrome Biology of Inflammatory Cancer Transformation (2021KJ03-12, China), the Innovative Research Team of High-level Local Universities in Shanghai (SHSMU-ZDCX20212702, China), and the Chinese Special Fund for State Key Laboratory of Bioreactor Engineering (2060204), Innovation Program of Shanghai Municipal Education Commission (2019-01-07-00-10-E00056, 2021-01-07-00-02-E00104, China), the Scientific and Technological Innovation Action Plan of Science and Technology Commission of Shanghai (20JC1411300, China). We are also grateful for the help of Prof. Jin Huang, Prof. Yi Sun, Dr. Qing Yu, and Dr. Zhiguo Hu.

Author contributions

Shuaishuai Ni, Jian Li and Lijun Jia conceived idea and designed experiments; Xin Chen and Shuaishuai Ni designed and synthesized the derivatives; Shuaishuai Ni, Lele Ding, Qian Liu, and Xi Wang performed the *in vitro* experiments; Xin Chen, Xianggang Mu, and Shuaishuai Ni performed the *in vivo* experiments; Xin Chen, Shuaishuai Ni, and Yixiang Xu analyzed the data;

Shuaishuai Ni and Xin Chen wrote the manuscript; Fei Mao and Jinlian Wei check the manuscript. All co-authors contributed comments. The authors declare no competing financial interests.

Conflicts of interest

The authors declare no conflict of interest.

Appendix A. Supporting information

Supporting data to this article can be found online at https://doi.org/10.1016/j.apsb.2023.11.004.

References

1. Dowling EC, Chawla N, Forsythe LP, de Moor J, McNeel T, Rozjabek HM, et al. Lost productivity and burden of illness in cancer survivors with and without other chronic conditions. *Cancer* 2013;**119**:3393–401.
2. Daher IN, Daigle TR, Bhatia N, Durand JB. The prevention of cardiovascular disease in cancer survivors. *Tex Heart Inst J* 2012;**39**:190–8.
3. Bodai BI, Tuso P. Breast cancer survivorship: a comprehensive review of long-term medical issues and lifestyle recommendations. *Perm J* 2015;**19**:48–79.
4. Siegel R, DeSantis C, Virgo K, Stein K, Mariotto A, Smith T, et al. Cancer treatment and survivorship statistics, 2012. *CA Cancer J Clin* 2012;**62**:220–41.
5. Curigliano G, Cardinale D, Dent S, Criscitiello C, Aseyev O, Lenihan D, et al. Cardiotoxicity of anticancer treatments: epidemiology, detection, and management. *CA Cancer J Clin* 2016;**66**:309–25.
6. Yeh ET, Tong AT, Lenihan DJ, Yusuf SW, Swafford J, Champion C, et al. Cardiovascular complications of cancer therapy: diagnosis, pathogenesis, and management. *Circulation* 2004;**109**:3122–31.
7. Chlebowski RT. Adriamycin (doxorubicin) cardiotoxicity: a review. *West J Med* 1979;**131**:364–8.
8. Azad NS, Posadas EM, Kwitkowski VE, Steinberg SM, Jain L, Annunziata CM, et al. Combination targeted therapy with sorafenib and bevacizumab results in enhanced toxicity and antitumor activity. *J Clin Oncol* 2008;**26**:3709–14.
9. Pradere U, Garnier-Amblard EC, Coats SJ, Amblard F, Schinazi RF. Synthesis of nucleoside phosphate and phosphonate prodrugs. *Chem Rev* 2014;**114**:9154–218.
10. Johnstone TC, Suntharalingam K, Lippard SJ. The next generation of platinum drugs: targeted Pt(II) agents, nanoparticle delivery, and Pt(IV) prodrugs. *Chem Rev* 2016;**116**:3436–86.
11. Ewer MS, Ewer SM. Cardiotoxicity of anticancer treatments. *Nat Rev Cardiol* 2015;**12**:620.
12. Zhan C, Miller MR. Excess length of stay, charges, and mortality attributable to medical injuries during hospitalization. *JAMA* 2003;**290**:1868–74.
13. Ashburn TT, Thor KB. Drug repositioning: identifying and developing new uses for existing drugs. *Nat Rev Drug Discov* 2004;**3**:673–83.
14. Pushpakom S, Iorio F, Eyers PA, Escott KJ, Hopper S, Wells A, et al. Drug repurposing: progress, challenges and recommendations. *Nat Rev Drug Discov* 2019;**18**:41–58.
15. Yu Q, Hu Z, Shen Y, Jiang Y, Pan P, Hou T, et al. Gossypol inhibits cullin neddylation by targeting SAG–CUL5 and RBX1–CUL1 complexes. *Neoplasia* 2020;**22**:179–91.
16. Yu Q, Jiang Y, Sun Y. Anticancer drug discovery by targeting cullin neddylation. *Acta Pharm Sin B* 2020;**10**:746–65.
17. Kamitani T, Kito K, Nguyen HP, Yeh ET. Characterization of NEDD8, a developmentally down-regulated ubiquitin-like protein. *J Biol Chem* 1997;**272**:28557–62.
18. Enchev RI, Schulman BA, Peter M. Protein neddylation: beyond cullin-RING ligases. *Nat Rev Mol Cell Biol* 2015;**16**:30–44.
19. Huang DT, Ayrault O, Hunt HW, Taherbhoy AM, Duda DM, Scott DC, et al. E2-RING expansion of the NEDD8 cascade confers specificity to cullin modification. *Mol Cell* 2009;**33**:483–95.
20. Bohnsack RN, Haas AL. Conservation in the mechanism of Nedd8 activation by the human AppBp1-Uba3 heterodimer. *J Biol Chem* 2003;**278**:26823–30.
21. Li L, Kang J, Zhang W, Cai L, Wang S, Liang Y, et al. Validation of NEDD8-conjugating enzyme UBC12 as a new therapeutic target in lung cancer. *EBioMedicine* 2019;**45**:81–91.
22. Li L, Wang M, Yu G, Chen P, Li H, Wei D, et al. Overactivated neddylation pathway as a therapeutic target in lung cancer. *J Natl Cancer Inst* 2014;**106**:dju083.
23. Soucy TA, Smith PG, Milhollen MA, Berger AJ, Gavin JM, Adhikari S, et al. An inhibitor of NEDD8-activating enzyme as a new approach to treat cancer. *Nature* 2009;**458**:732–6.
24. Lu P, Liu X, Yuan X, He M, Wang Y, Zhang Q, et al. Discovery of a novel NEDD8 activating enzyme inhibitor with piperidin-4-amine scaffold by structure-based virtual screening. *ACS Chem Biol* 2016;**11**:1901–7.
25. Zhong HJ, Wang W, Kang TS, Yan H, Yang Y, Xu L, et al. A Rhodium(III) complex as an inhibitor of neural precursor cell expressed, developmentally down-regulated 8-activating enzyme with *in vivo* activity against inflammatory bowel disease. *J Med Chem* 2017;**60**:497–503.
26. Smith SM, Huo T, Delia Johnson B, Bittner V, Kelsey SF, Vido Thompson D, et al. Cardiovascular and mortality risk of apparent resistant hypertension in women with suspected myocardial ischemia: a report from the NHLBI-sponsored WISE Study. *J Am Heart Assoc* 2014;**3**:e000660.
27. Smith CD, Wang A, Vembaiyan K, Zhang J, Xie C, Zhou Q, et al. Novel carvedilol analogues that suppress store-overload-induced Ca^{2+} release. *J Med Chem* 2013;**56**:8626–55.
28. Bhalla KN, Fiskus W. NEDD8 and HDACs: promising cotargets in AML. *Blood* 2016;**127**:2168–70.
29. McMillin DW, Jacobs HM, Delmore JE, Buon L, Hunter ZR, Monrose V, et al. Molecular and cellular effects of NEDD8-activating enzyme inhibition in myeloma. *Mol Cancer Ther* 2012;**11**:942–51.
30. Walden H, Podgorski MS, Huang DT, Miller DW, Howard RJ, Minor Jr DL, et al. The structure of the APPBP1-UBA3-NEDD8-ATP complex reveals the basis for selective ubiquitin-like protein activation by an E1. *Mol Cell* 2003;**12**:1427–37.
31. Schaefer WH, Politowski J, Hwang B, Dixon Jr F, Goalwin A, Gutzait L, et al. Metabolism of carvedilol in dogs, rats, and mice. *Drug Metab Dispos* 1998;**26**:958–69.
32. Stanek M, Picard LP, Schmidt MF, Kaindl JM, Hübner H, Bouvier M, et al. Hybridization of β-adrenergic agonists and antagonists confers G protein bias. *J Med Chem* 2019;**62**:5111–31.
33. Hieble JP, Bondinell WE, Ruffolo Jr RR. Alpha- and beta-adrenoceptors: from the gene to the clinic. 1. molecular biology and adrenoceptor subclassification. *J Med Chem* 1995;**38**:3415–44.
34. Lin S, Liu J, Li H, Liu Y, Chen Y, Luo J, et al. Development of highly potent carbazole amphiphiles as membrane-targeting antimicrobials for treating gram-positive bacterial infections. *J Med Chem* 2020;**63**:9284–99.
35. Nakamura K, Kusano K, Nakamura Y, Kakishita M, Ohta K, Nagase S, et al. Carvedilol decreases elevated oxidative stress in human failing myocardium. *Circulation* 2002;**105**:2867–71.
36. Yue TL, Cheng HY, Lysko PG, McKenna PJ, Feuerstein R, Gu JL, et al. Carvedilol, a new vasodilator and beta adrenoceptor antagonist, is an antioxidant and free radical scavenger. *J Pharmacol Exp Ther* 1992;**263**:92–8.
37. Lopaschuk GD, Karwi QG, Tian R, Wende AR, Abel ED. Cardiac energy metabolism in heart failure. *Circ Res* 2021;**128**:1487–513.
38. Raju TN. The Nobel chronicles. 1988: James Whyte black, (b 1924), Gertrude elion (1918-99), and George H Hitchings (1905-98). *Lancet* 2000;**355**:1022.
39. Ni S, Wei H, Li B, Chen F, Liu Y, Chen W, et al. Novel inhibitors of staphyloxanthin virulence factor in comparison with linezolid and vancomycin *versus* methicillin-resistant, linezolid-resistant, and

vancomycin-intermediate *Staphylococcus aureus* infections *in vivo*. *J Med Chem* 2017;**60**:8145−59.
40. Ni S, Chen X, Yu Q, Xu Y, Hu Z, Zhang J, et al. Discovery of candesartan cilexetic as a novel neddylation inhibitor for suppressing tumor growth. *Eur J Med Chem* 2020;**185**:111848.
41. Chen X, Yang X, Mao F, Wei J, Xu Y, Li B, et al. Development of novel benzimidazole-derived neddylation inhibitors for suppressing tumor growth *in vitro* and *in vivo*. *Eur J Med Chem* 2021;**210**:112964.
42. Huang Y, Xu Y, Song R, Ni S, Liu J, Xu Y, et al. Identification of the new covalent allosteric binding site of fructose-1,6-bisphosphatase with disulfiram derivatives toward glucose reduction. *J Med Chem* 2020;**63**:6238−47.
43. Wilson BE, Jacob S, Yap ML, Ferlay J, Bray F, Barton MB. Estimates of global chemotherapy demands and corresponding physician workforce requirements for 2018 and 2040: a population-based study. *Lancet Oncol* 2019;**20**:769−80.